Eng. Sci., 2021, **16**, 47–70

Engineered Science

DOI: https://dx.doi.org/10.30919/es8d552

An Overview of Advanced Nanomaterials for Sensor Applications

Deepak Rohilla,[1] Savita Chaudhary[2,*] and Ahmad Umar[3, 4,*]

Abstract

Because of their superior optical, luminescent, catalytic, magnetic, and electrical characteristics, nanomaterials have shown great promise in the realm of sensing. The potential to establish better control over the analytical performance of formed sensors is due to the simplicity of manufacturing and adjustable characteristics of a broad variety of nanomaterials. Herein, a comprehensive review on carbon-based quantum dots, noble metals (Au, Ag, Pt), and other metal, metal oxide and sulphides based nanoparticles including ZnO, CeO_2, TiO_2, SnO_2, ZrO_2, CdS, CdSe, CuS, CuO, ZnS, WO_3, Cr_2O_3, Gd_2O_3, Yb_2O_3-based electrochemical, optical, fluorescence, and pH-dependent sensors for detecting harmful metal ions (Hg^{2+}, Pb^{2+}, Cd^{2+}), and so on are discussed. This review also discusses the utilization of different nanomaterials to fabricate enzymatic and non-enzymatic electrochemical sensors. Sensors to detect agrochemical contaminants and other hazardous materials are also discussed. Finally, the future perspectives and current challenges in achieving large-scale commercialized nanomaterials-based sensors are reviewed.

Keywords: Advanced Nanomaterials; Sensor.
Received: 1 October 2021; Accepted: 14 October 2021.
Article type: Review article.

1. Introduction

Due to the nanoscale dimension, nanomaterials exhibit exceptional properties that differ from those of their bulk counterparts.[1-4] Nanomaterials have a high surface-to-volume ratio, resulting in a wide range of chemical, mechanical, optical, and magnetic properties.[5,6] To adequately investigate the properties and applications of nanomaterials, it is necessary to classify them. However, numerous factors can be considered while classifying nanomaterials, such as physical and chemical properties, dimensionality, production method, composition, homogeneity and so forth.[7-8] Nanomaterials can be classified into 0D, 1D, 2D, and 3D nanostructures depending on the dimensionality (D) of their features.[9] 0D nanostructures, mainly include quantum dots, nanospheres, single molecules and atoms, with tiny point formations in all dimensions.[10,11]

1D nanostructures, such as nanotubes and nanowires, are non-nanoscale structures having only one dimension. 2D nanostructures such as nanoplates, nanosheets, nanodiscs and nanobelts are two-dimensional structures in nanoscale.[12,13] Finally, three-dimensional nanostructures such as nanocombs, nanoflowers, and nanotetrapods are arbitrary structures with nanoscale characteristics in any of the three dimensions.[14-15] Thus, nanomaterials are extremely advantageous in a variety of nanotechnology domains, including nanochemistry, nanoelectronics, nanophotonics, optoelectronics, bioelectronics, biomedicine, nanobiotechnology, nanomechanics, biochemistry, and electrochemistry.[16-18] These enable a diverse range of applications, including quantum-effect, lasers, cells, solar cells, transistors, catalysts, molecular electronic devices, photonic band gap devices, photocatalysts, nanofuel cells, surface enhanced Raman spectroscopy (SERS), nanodrug delivery systems, nanoactuators, advanced energy storage devices, and nanosensors.[19-21] Currently, large number of advanced nanomaterials have also been used for fabricating diverse range of sensors for detecting harmful toxins in ecosystem.

[1] *Department of Chemistry, RPS Degree College, Balana, Mohindergarh, Haryana 123029, India.*
[2] *Department of Chemistry and Centre of Advanced Studies in Chemistry, Panjab University, Chandigarh 160014, India.*
[3] *Department of Chemistry, College of Science and Arts, Najran University, Najran-11001, Kingdom of Saudi Arabia.*
[4] *Promising Centre for Sensors and Electronic Devices (PCSED), Najran University, Najran-11001, Kingdom of Saudi Arabia.*
**Email:* schaudhary@pu.ac.in (S. Chaudhary), ahmadumar786@gmail.com (A. Umar)

© Engineered Science Publisher LLC 2021

To briefly introducing the term, these nanosensors are the devices that detect and respond to changes in its immediate environment. When compared to conventional sensors, nanosensors can detect chemicals, viruses, infections and even a single chemical element at a scale of 1–100 nanometers.[22,23] The main advantages of nanosensors include their high speed, mobility, and low cost in mass production, as well as their ability to detect minute sample volumes. Recently, the application of nanosensor in real world has shown significant up gradation due to ease in fabrication and usage of easy instruments for detecting their signals. In addition, the application of nanomaterials in sensor fabrication has also emphasized over the miniaturization of instruments and allowed to unite them with other system for toxin sensing. The applications of advanced nanosensor in health care systems have enhanced their scope in fabricating advanced biomarkers for forensic applications. The nanosensors have also been used for observing the biochemical analytes in living systems and further enhanced their usage in various biomedical applications.

The last decade has witnessed the significant production of different types of nanosensors for diverse range of toxins. The higher interest in their production and utilization is mainly aroused due to two major reasons. First and the foremost reason is their superior performance. Nanosensors have persuaded the world due to their successful usage in a variety of applications ranging from the hazardous gas detection in fire and food industry, to highly sophisticated applications such as advanced medical and military applications.[24-26] The second reason of their popularization include the higher rate of innovation in the fabrication methods for producing nanosensors with quick response rate with higher sensitivity and selectivity.[27-29] Numerous nanostructured materials and composites have been developed for producing different range of sensing platforms by using a variety of different preparation processes for different range of sensing applications.[30, 31] For example, chemosensitive gas sensors with high sensitivity have been widely produced by using metal oxide nanostructures such as SnO_2 nanowires, ZnO nanotetrapods, and TiO_2 nanorods.[32-34] Additionally, extremely sensitive electrochemical biosensors relying on the confluence of biocompatible materials such as antibodies, DNA, and enzymes with novel electrode materials such as metal/carbon/metal oxide/conductive polymer nanostructures and nanocomposites of gold nanoparticles, carbon nanotubes, graphene, carbon nanotubes/gold, carbon nanotubes/ZnO.[35-39] Herein, a comprehensive review on carbon-based quantum dots, noble metals (Au, Ag, Pt), and other metal, metal oxide and sulphides based nanoparticles including ZnO, CeO_2, TiO_2, SnO_2, ZrO_2, CdS, CdSe, CuS, CuO, ZnS, WO_3, Cr_2O_3, Gd_2O_3, Yb_2O_3-based electrochemical, optical, fluorescence, and pH-dependent sensors for detecting harmful metal ions (Hg^{2+}, Pb^{2+}, Cd^{2+}) has been discussed. The nanomaterial-based gas and chemical sensors for environmental science and technology application has been discussed in detail. The nanomaterials-based sensor in health and food technological area has also been discussed in this review. This work could explore a new horizon to fabricate advanced sensors for checking environmental issues.

2. Advanced metal oxide-based sensors

2.1. Gas and chemical sensors for environmental science and technological applications

The release of harmful gases and excessive usage of chemicals have possessed harmful effect on living beings. Sometime the leakage of gases has caused severe damage to mankind. Therefore, the development of sensors for checking such leakage of gases is found to be useful for the society. Till date, large number of materials was employed for the fabrication of gas sensors. In addition, the chemiluminescence behavior of nano materials *i.e.* release of light or changes in intensity during interacting with analytes has also been used for developing the highly effective nanosensor for detecting harmful toxin in our environment. The used nanomaterials for fabricating the sensors were either produced using the hydrothermal methods or by using the wet chemical reactions. In certain cases, the fast synthetic methodologies such as microwave assisted process have also been used for the preparation of advanced nanomaterials for preparing nanosensors. These used methodologies have possessed better control over the morphology and the sizes of the prepared nanomaterials as compared to the conventionally used handicraft-like brush printing and drop casting techniques for preparing gas sensors. For instance, Song *et al*. have described the fabrication of highly sensitive gas sensors using a TiO_2 nanoparticle-spaced reduced graphene oxide (RGO) assembly.[41] The used TiO_2 nanospacers were formed by intercalating a 2D MXene between RGO sheets. The major advantage of using GO and MXene is the existence of negative zeta potential charge of −45.68 and −41.29 mV, respectively. As a result, they have the higher tendency to form a stable- and highly uniform mixed colloidal solution. Through drop casting method they are easily deposited over the surface of electrode. The incorporation of GO with MXene nanosheets, resulted in the variation in the diffraction peaks of graphene oxide at 11.8°. This behavioral shift was explained due to the increment in the interlayer distance of particles from 0.75 to 1.14 nm. The TiO_2-spaced RGO assembly has a homogeneous distribution of nanoparticles and highly crumpled RGO sheets that interconnect via micrometer-scale pores (Fig. 1). The measurements were done by taking the pure RGO as a reference system. Due to the increased accessible surface area and active adsorption sites, the selectivity of the TiO_2-spaced RGO sensor to NO_2 increased by over 400% when compared to pure RGO (Fig. 1a). The developed sensor have possessed higher rate of sensitivity for NO_2 gas by using the home made gas sensing system. For the fabrication of sensor, the formed material was placed in the quartz chamber having the fixed inlet and outlet for gas molecules. The respective amount of gas capacity was adjusted by using the external mass-flow

 © Engineered Science Publisher LLC 2021

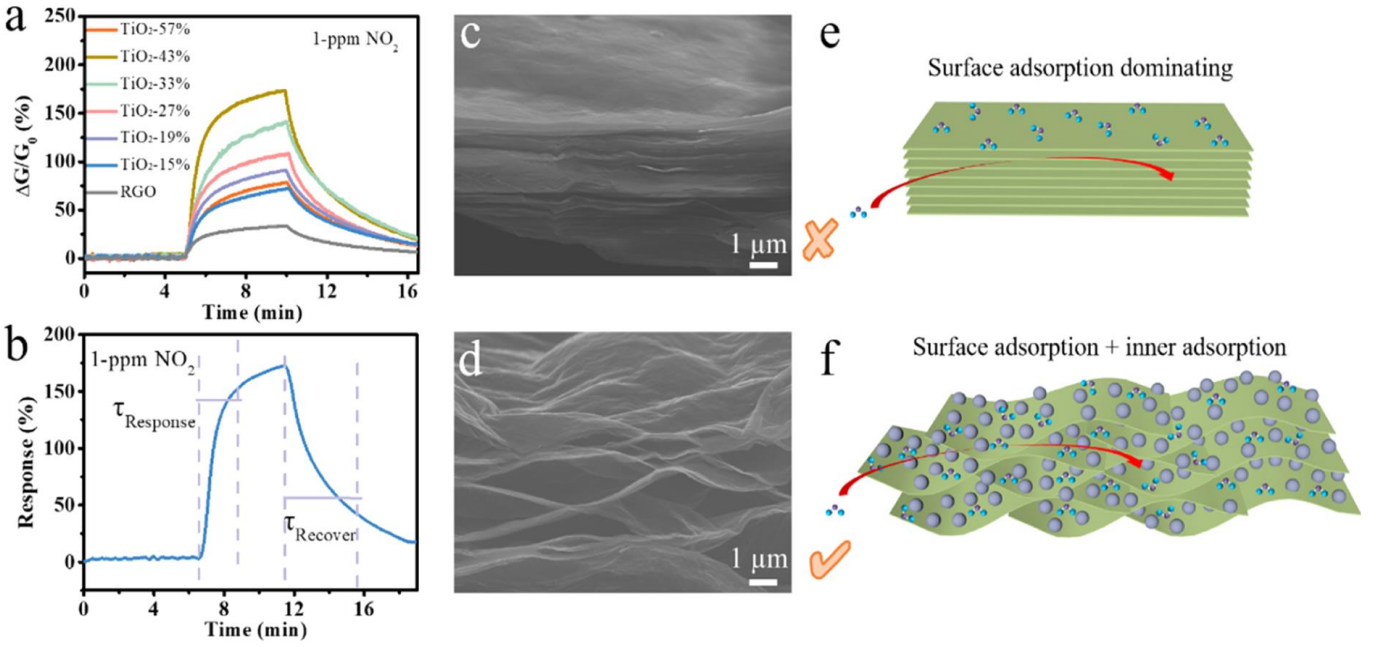

Fig. 1 (a) Dynamic sensing response of TiO_2-spaced RGO with different compositions with GO as a reference. (b) Response and recovery times defined for TiO_2-spaced RGO sensing for 1 ppm of NO_2. (c, d) Cross-sectional SEM images of the pure RGO film (c) and TiO_2-spaced RGO film (d). (e, f) Schematic illustration of the pure RGO film (e) and TiO_2-spaced RGO film (f) upon exposure to the NO_2 target. Reproduced with the permission from [41], Copyright 2021, American Chemical Society.

controllers. The dilution gases used during the analysis were N_2 or dry air with flow rate of 500 scan rate. The configuration having two electrodes was employed for sensing the presence of NO_2 gas with constant bias of 1 V over the sensor. The response rate was estimated by varying the current values at 25 °C ± 1 °C.

The response behavior of the chosen sensor is defined by using the following equation:

$$R = \Delta G/G_0 \times 100\% \quad (1)$$

Here, ΔG is defined as the relative change in the conductance value after purging the target gas. However, the G_0 is known as the conductance of reference gases used during analysis. The sensing performance towards NO_2 gas was further affected by varying the amount of TiO_2 from 15−57% in the reaction medium (Fig. 1a). It has been observed that the NO_2 response increased linearly with increasing the concentration of TiO_2 in the reaction medium from 15 to 43% (Fig. 1b). These changes in the measurements were mainly explained due to the enhancement of the interlayer distance between the two, which further eases the infiltration and adsorption of gas molecules over the surface (Figs. 1c and 1d). The surface adsorption as well as inner adsorption is mainly responsible for the sensing of NO_2 (Figs. 1e and 1f). In addition the selectivity of the sensor was tested in presence of gases such as NO, NH_3, SO_2, O_2, CO_2. In addition, different types of volatile organic compound such as acetone, methanol and ethanol have also been tested to verify the performance of developed sensor. On interpreting the results, it was found that except for NO_2, the developed sensor also displayed a response behavior of 55% towards 1 ppm of NO. However, the response intensity ratio of target gas *i.e.* NO_2 to NO was found to be 3:1. The results verified the sensitivity of the formed sensor and displayed high prospective role in developing wearable and practical gas sensor for industrial purpose.

The copper (II) oxide (CuO) nanoparticles have been synthesized using the cost-effective and simple hydrothermal synthetic approach for producing the chemiresistive sensor for detecting Volatile Organic Compounds (VOCs).[42] These findings suggest that a chemiresistive sensor based on CuO-NPs is optimal for qualitative detection of benzene, toluene, ethylbenzene, and xylene (BTEX) chemical vapors (*i.e.* Benzene, Toluene, Ethylbenzene, and Xylene). The formation of the sensor was done by coating the powdered slurry of CuO-NPs with deionized water over the exterior surface of alumina ceramic tube of length of 4 mm with internal diameter of 0.8 mm and external diameter of 1.2 mm. In addition Au electrodes separated by 1 mm distance has already been fixed over the surface through Au paste. The contact between the two electrodes was further made by using two Pt wires. The resultant sensor acts as a chemiresistive sensor for VOCs. For quantification of data, the circuit voltage (Vc) of the system was maintained 5V. The formed gas sensor (R_s) is further attached in series with an external load resistor (R_L). However, the output voltage (V_{output}) was kept as a terminal voltage of the load resistor (R_L). The temperature during the measurement was controlled by controlling the heating voltage (V_H). Further, the resistance of the formed sensor *i.e.* resistance (R_s) was calculated by the following equation:

$$R_s = (V_c - V_{output})/V_{output} \times 100 \quad (2)$$

The rapid and sensitive hydrogen sulphide (H_2S) sensors has also been produced by using NiO/WO_3 nanoparticles (NPs)

© Engineered Science Publisher LLC 2021

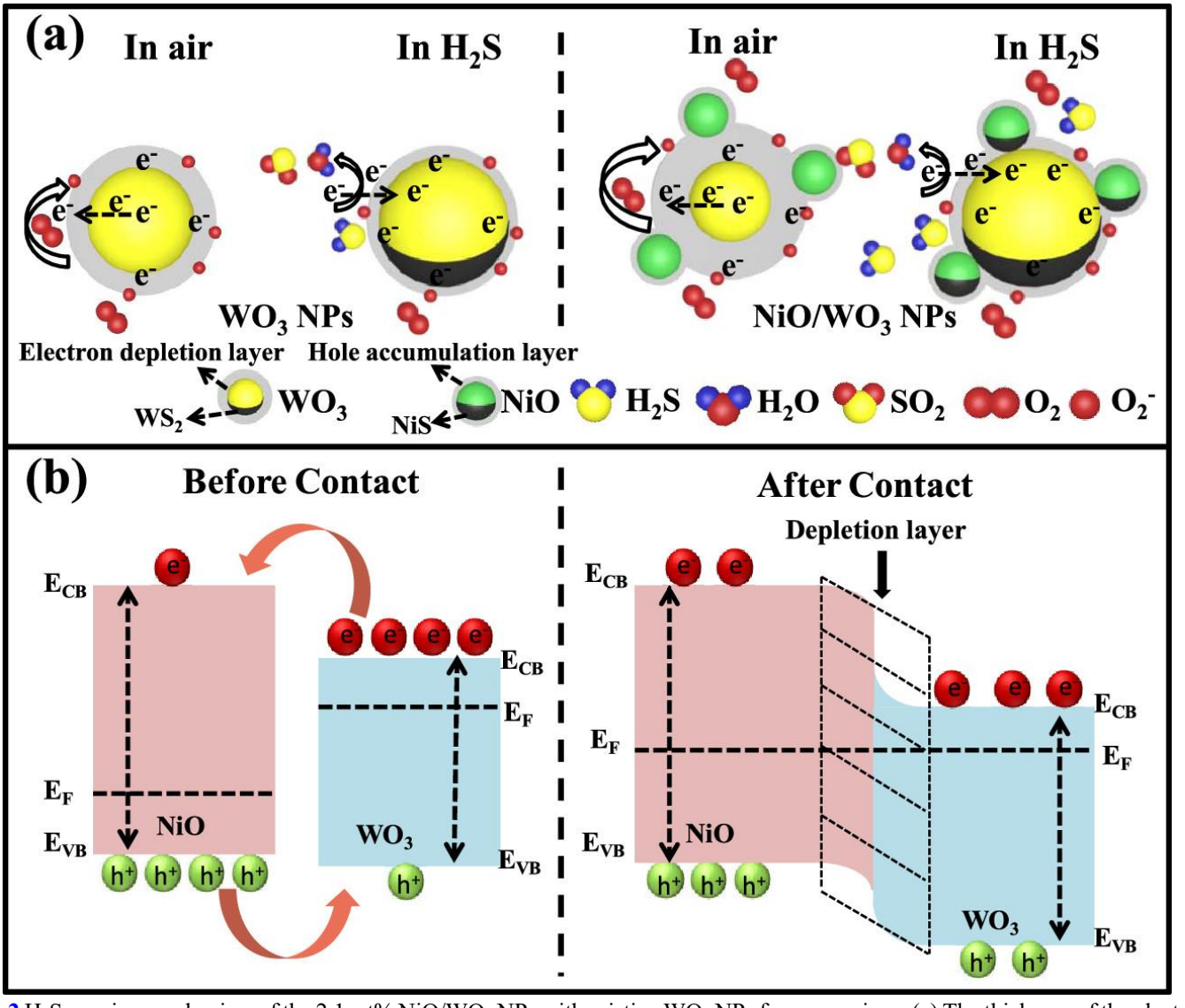

Fig. 2 H_2S-sensing mechanism of the 2.1 wt% NiO/WO_3 NPs with pristine WO_3 NPs for comparison. (a) The thickness of the electron depletion layer varies in air and H_2S environment. (b) The semiconducting band bending before and after the NiO/WO_3 contact. Reproduced with the permission from [43], Copyright 2021, American Chemical Society.

generated by hydrolyzing WO_3 NPs and then decorating with NiO NPs (Fig. 2) via a hydrothermal method.[43] The formation of the sensor was done by grounding the mixture of WO_3 NPs with NiO/WO_3 nanoparticles in presence of terpilenol. The resultant slurry was further on the surface of a ceramic tube. The ceramic tube was further assembled with Au electrodes and Pt wires for forming the chemiresistive circuit. The complete drying of the surface was done at 60 °C for 2 h. Further the ceramic tube was welded over the hexagonal socket. The Ni−Cr alloy, was used as a heating wire in a ceramic tube. The temperature of the system was controlled by applying the external voltage. Further the target gases were purged at 200 °C for 48 h, and sensing measurements were done (Fig. 2a). The sensor response was estimated by using the following equation:

$$S = R_A/R_g \quad (3)$$

where R_A and Rg are defined as the resistances in air and target gas, respectively. The main mechanism during the sensing involves adsorption of target gas molecules over the surface of semiconducting nanomaterials which further affects the band bending in WO_3 NPs and lead to the variations in the resistance value (Fig. 2b). The reactive oxygen species were formed over the surface of WO_3 NPs via adsorbed of atmospheric oxygen gas. These O_2 gas molecules have the tendency to capture free electrons from the conduction band of WO_3 NPs (Fig. 2a). The equations are explained below:

$$O_2\,(gas) \rightarrow O_2\,(ads) \quad (4)$$

$$O_2\,(ads) + e^- \rightarrow O_2^-\,(ads) \quad (5)$$

$$2H_2S + 3\,O_2^- \rightarrow 2SO_2 + 2\,H_2O + 3e^- \quad (6)$$

Furthermore, the weight percentage variations have also affected the measurements. It was observed that 2.1 wt% NiO/WO_3 NPs exhibit a significant sensitivity to H_2S (R_a/R_g = 150311370 @ 10 ppm, 100 °C), which is 42.6-fold greater than that of pure WO_3 NPs (R_a/R_g = 3535.6 @ 10 ppm, 100 °C) (Fig. 2a). Additionally, the H_2S sensor exhibits a detection limit of around ppb (Ra/Rg = 4.952.9 @ 0.05 ppm, 100 °C)

© Engineered Science Publisher LLC 2021

with excellent selectivity.

To detect carbon oxides, researchers have also used Al and Mg co-doped ZnO nanoparticles produced by using the sol-gel process.[44] The development of the sensor was done by coating the aqueous slurry of Al, Mg co-doped ZnO nanoparticles on alumina substrates with having dimensions of 3 mm×6 mm. The substrate was further paired up with the Pt electrodes and a heating element from the back side. The estimation of the electrical resistance was done via using a multimeter data acquisition unit (Agilent 34,970 A). The response behavior of the gas was measured by using equation 3. It has been found that the sensing aptitude of the sensor has been significantly affected by the changes in the structural, morphological, and optical features of Al and Mg. Finally, it was established that Al-Mg co-doping on ZnO films has further improved the sensing capabilities toward carbon oxides in terms of response, detection limit, and recovery time when compared to undoped ZnO films. It has been observed that the existence of stacking defect with higher surface roughness and increased value of surface to volume ratio is mainly responsible factor for the detection of gas molecules. In addition the existence of detects over the external surface of Al-Mg doped ZnO samples has further supported the adsorption of oxygen on active centers. Moreover, the existence of donor defect on Al-Mg doped ZnO samples has further supported the interaction of CO with oxygen species. This mechanism is easily explained by the following equation:

$$D \leftrightarrow D^{+} + e^{-} \quad (7)$$

The interactions of these oxygen species with target gas molecules *i.e.* CO and CO_2 molecules have further enhanced the sensitivity of the formed sensor. Furthermore, the developed sensor has displayed the resistance change on exposing the surface with different concentrations of CO. Xu has use the application of 4-(((3-aminonaphthalen-2-yl) amino)methyl)benzoic acid (DAN-1-functionalized CdTe/CdS/ZnS quantum dots (QDs@DAN-1), for producing a simple, direct fluorescence based sensor for the simultaneous determination of nitric oxide and hydrogen sulfide in a sample (Fig. 3).[45] DAN-1 could selectively identify nitric oxide in the formed sensor and produce highly luminous naphtho triazole (DAN-1-T). Meanwhile, hydrogen sulfide has produced quenching effect on the fluorescence intensity of the QDs (Fig. 3). The QDs and DAN-1-T were stimulated synchronously at 365 nm and emitted at maximum wavelengths of 635 and 440 nm, respectively. Nitric oxide and hydrogen sulfide concentrations have been evaluated concurrently by using two distinct fluorescence signals. Nitric oxide and hydrogen sulfide has possessed the detection limits of 0.051 and 0.13 M, respectively.

Zhou *et al*. proposed a template-free strategy for fabricating tin oxide (SnO_2) porous hollow microsphere (PHMs) by exploiting the competitive pressures between solvent evaporation rate and phase separation dynamics of colloidal SnO_2 quantum wires (Fig. 4a).[46] The wire formation was explained via the following equations.

$$SnCl_4.5H_2O + xRCOOH \rightarrow Sn(RCOOH)_xCl_{4-x}\cdot yH_2O + xHCl(g) + (5-y)\ H_2O\ (g) \quad (8)$$

$$Sn(RCOOH)_xCl_{4-x} + H_2O \rightarrow SnO_2\ (NCs) + RCOOH \quad (9)$$

$$Sn(RCOOH)_xCl_{4-x} + R'OH \rightarrow SnO_2\ (NCs) + RCOOR \quad (10)$$

$$SnO_2\ (NCs) + RCOOH + RNH_2 \rightarrow [SnO_2](RCOO)(RNH_2) \quad (11)$$

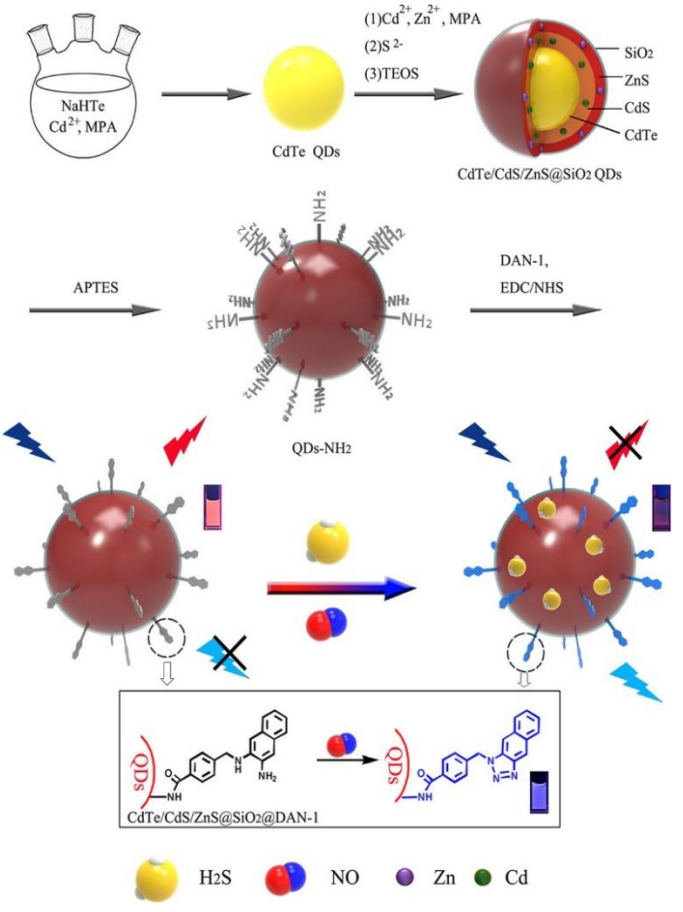

Fig. 3 Schematic Illustration of QDs@DAN-1 Synthesis and the Principle of the Sensor to Determine NO and H_2S. Reproduced with the permission from [45]. Copyright 2021, American Chemical Society.

The SnO_2 PHMs have possessed a high degree of structural firmness (Fig. 4a) and processing suitability with a variety of substrates. This permits the development of improved response and recovery rate of NO_2 gas sensors at ambient temperature (Fig. 4a). The gas sensing was mainly performed by using the commercial WS30A testing system. The measurements were carried out at a direct current (DC) voltage of 5 V. The working temperature was kept at 25 ± 2 °C, and the relative humidity during the measurement was fixed at 58–62%. The formation of the sensor was mainly done by the electro spraying method. The presence of hollow spheres of SnO_2 has further restricted the agglomeration of particles during sensing activity (Fig. 4b). The enhanced NO_2-sensing property is a result of efficient gas adsorption competition

© Engineered Science Publisher LLC 2021

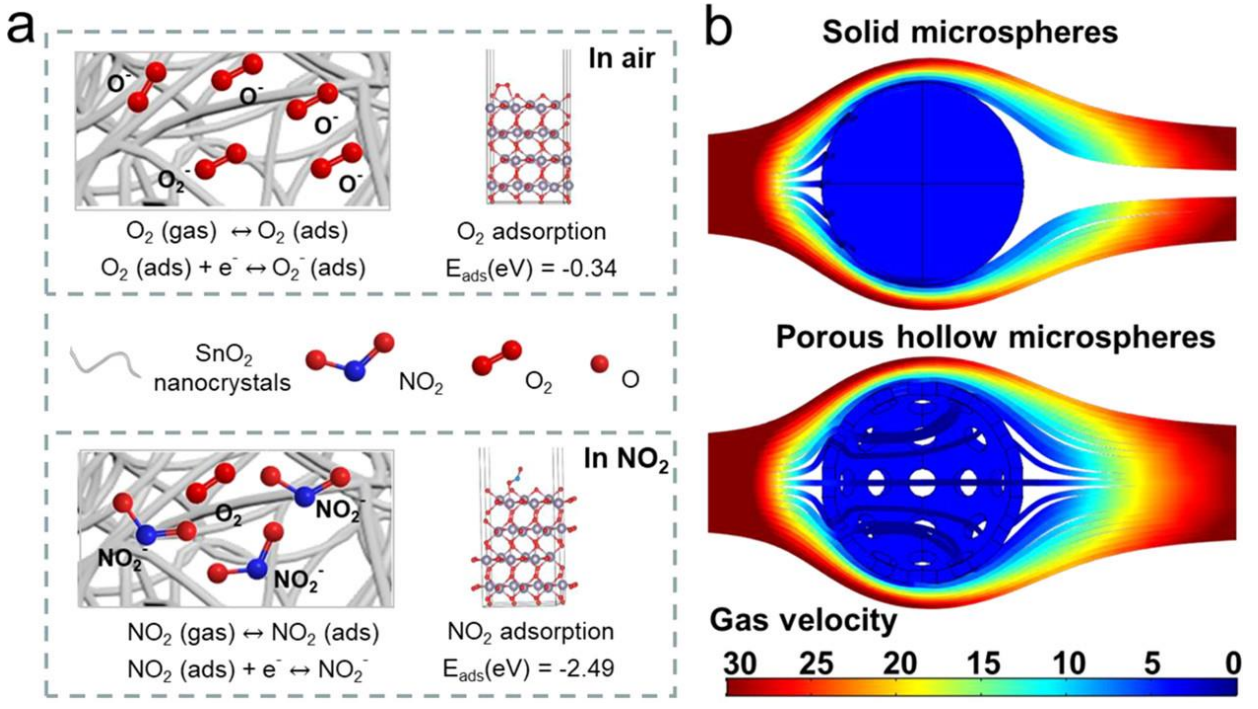

Fig. 4 (a) Schematic NO_2-sensing mechanism of the SnO_2 PHM sensors. (b) COMSOL simulation of gas velocity at the solid and porous hollow microspheres. Reproduced with the permission from [46]. Copyright 2021, American Chemical Society.

on solid surfaces with efficient diffusion channels, which improves the interaction of metal oxide solids with gas molecules in terms of transducer function, receptor function, and utility factor (Fig. 4b). The sensor response behavior has also been affected by the humidity in the reaction medium. At higher humidity, the water molecule has the tendency to get adsorbed over the surface of hollow SnO_2 and further dissociated into hydroxyl ions. These formed ions have provided the extra electrons to hollow SnO_2 particles and decreased the baseline resistance of the system. Moreover, these NO_2 gas molecules have possessed the oxidative nature with high electron affinity. Therefore, the presence of NO_2 gas molecules leads to reduction in the concentration of charge carriers over the surface of SnO_2.

The low temperature solution technique was effectively used to manufacture monophasic ZrO_2 nanoparticles for producing efficient gas sensors.[47] ZrO_2 nanoparticles demonstrated has owned a higher rate of gas sensing properties when exposed to carbon monoxide at a concentration of 50 ppm and a minimum working temperature of 240 °C. The excellent sensing properties can be attributed to the substantial oxygen surface vacancies available and the huge surface area of the ZrO_2 nanoparticles, which is advantageous for both the transportation and sensing processes of gas molecule. Jeon demonstrated that microwave-assisted surface modification of zinc oxide nanoflowers (ZnO NFs) with palladium nanoparticles (Pd NPs) enables the fabrication of high-performance chemiresistive-type hydrogen (H_2) gas sensors that operate at room temperature (RT) (Figs. 5a and 5b).[48] The synthesis of the advanced nanomaterials used for the fabrication of gas sensor was prepared using the advanced microwave assisted methodology. The reaction conditions have influenced the morphology of the formed particles. By influencing the reaction parameters, the formed nuclei of Zno NPs have the ability to transform them to flower shaped particles and further enhanced the surface area of the formed particles and supported their high performance activities in gas sensor. These particles have the higher adsorption sites available for the gas molecules to get attached over the nanosensors and give better response behavior towards sensing (Figs. 5c and 5d). The designed gas sensors have a significant response rate of up to 70% at 50 parts per million (ppm) and a theoretical detection limit of 10 parts per billion (ppb). Remarkably sensitive and sensitive ZnO-based gas sensors capable of detecting H_2 gas molecules at 300 ppb at room temperature with a response/recovery time of less than 3 minutes and a remarkable selectivity for other gases such as oxygen, nitric oxide and carbon monoxide (Figs. 5e and 5f). The pristine structure of Zno NPs and their compositional changes were further verified by using the X-ray photoelectron spectroscopy (XPS) analysis and it has further been verified that this prisitne structure has provided the conductive channels for making is better sensor for gas molecules (Figs. 5g and 5h).

The synthesis of a novel luminous material composed of silica nanoparticles functionalized with a terbium (Tb^{3+}) complex of a polyamino polycarboxylic chelator has possessed significant ability of fluorescence and has a higher potential towards the sensing of metal ions in aqueous and organic media.[49] Currently, the silver and gold nanoparticles have been modified by using Syzygium aromaticum bud extract for forming effective sensors.[50] For instance, Silver

 © Engineered Science Publisher LLC 2021

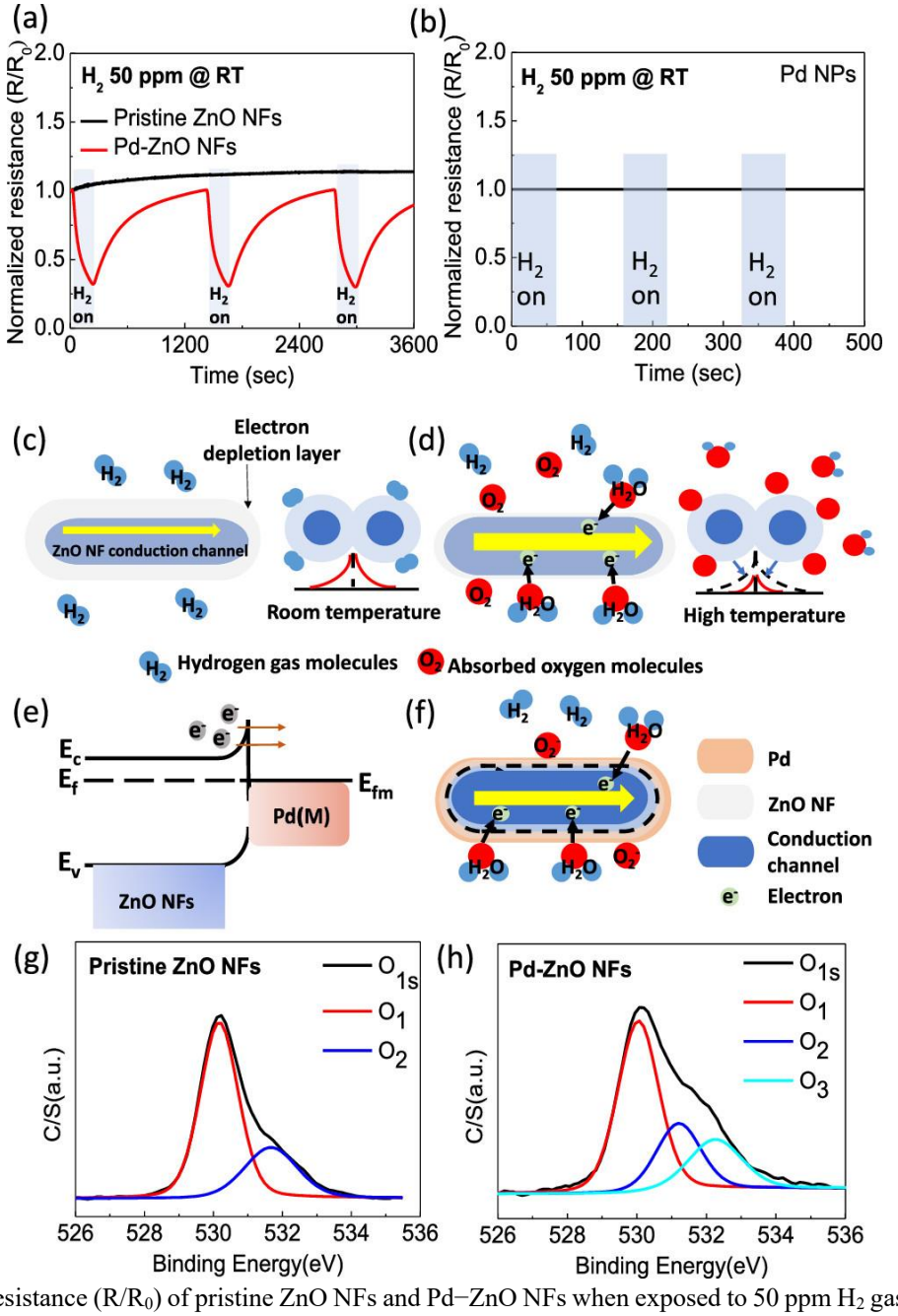

Fig. 5 (a) Normalized resistance (R/R_0) of pristine ZnO NFs and Pd−ZnO NFs when exposed to 50 ppm H_2 gas at RT. (b) Normalized resistance of Pd NPs when exposed to 50 ppm H_2 gas at RT. Electrical characteristics of ZnO NF conduction channel after reaction with H_2 gas molecules at (c) RT and (d) high temperatures. (e) Energy band diagram of the heterojunction between ZnO NFs and Pd NPs. (f) Sensing mechanism of the proposed H_2 gas sensors operating at RT. High-resolution XPS spectra for the O1s core level of (g) pristine ZnO NFs and (h) Pd−ZnO NFs. Reproduced with the permission from [48]. Copyright 2021, American Chemical Society.

nanoparticle (CAgNPs) have higher sensitivity for Hg(II) ions in aqueous solution, whereas gold nanoparticle (CAuNPs) were found to be sensitive for Cr(III) and Pb(II) ions. Hg(II) has a detection limit of 10 µm with CAgNPs, while Cr(III) and Pb(II) have a detection limit of 0.25 mm and 1 mm, respectively. Liu *et al.* suggested a quick, low-cost, and substantial approach for synthesizing chromium oxide nanoparticles (Cr_2O_3 NPs) by microwave heating by using Cr^{3+} ions with citrate for a few minutes (Fig. 6).[51] The citrate-coated Cr_2O_3 NPs can be combined with biomolecules (DNA) and used further for fluorescent bio sensing of mercury ions. The developed sensor has also possessed a complicated molecular logic computing system. The Hg^{2+} assay demonstrated broad linear ranges (0.21–2 and 4.2–50.5 M) with a low detection limit (5.78 nm), and excellent recovery rates in real- water samples. Additionally, by utilizing the interaction of matter and fluorescence energy in the Cr_2O_3 NPs-based sensing system, molecular logic gate operations ranging from simple (NOT, AND, OR and YES gates) to complicated circuits can be performed.

The application of advanced nanomaterials has owned solution phase precipitation production of ZnO nanoparticles

© Engineered Science Publisher LLC 2021

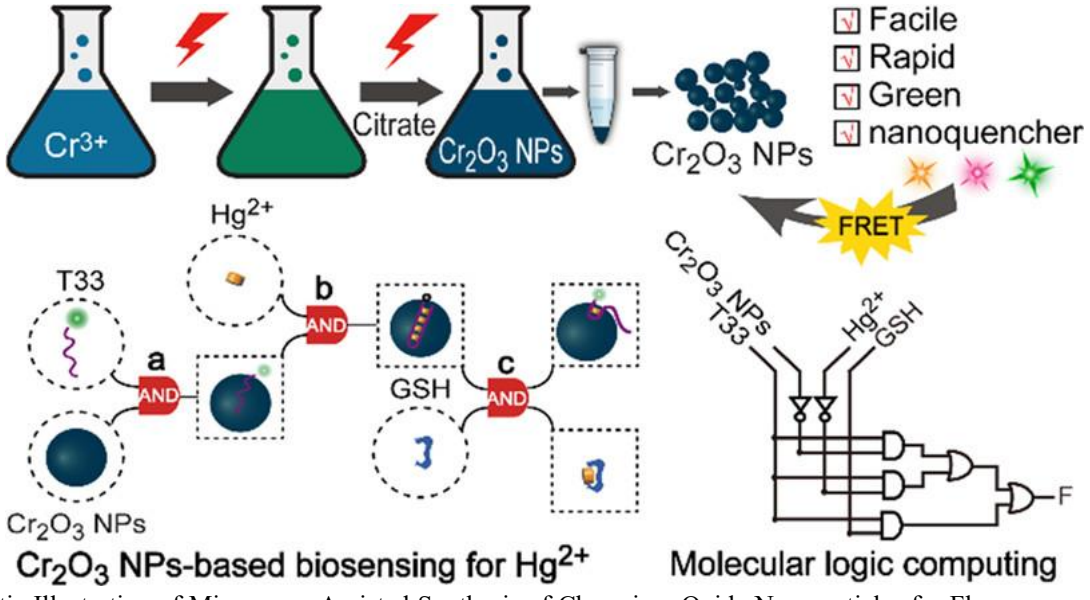

Fig. 6 Schematic Illustration of Microwave-Assisted Synthesis of Chromium Oxide Nanoparticles for Fluorescence Biosensing of Mercury Ions and Molecular Logic Computing. Reproduced with the permission from [51]. Copyright 2021, American Chemical Society.

doped with various amounts of lanthanum (La), namely 1, 5, and 10% mol percent for producing sensor.[52] Additionally, the fabricated nanoparticles have been employed as a fluorescent sensor for fluorescence detection of picric acid (PA). Surprisingly, the 1 mol% nanoparticles evidenced the highest sensitivity, *i.e*. the lowest limit of detection (LOD) value (1.05 M L^{-1}), toward PA, as matched to the 5 and 10 mol% (1.38 M L^{-1}) La-doped ZnO nanoparticles.

Li and his research group described a colorimetric sensor array for discriminating between different types of alkaloids.[53] The sensor array is based on the etching of two types of nanomaterials (Au@MnO_2 nanoparticles and MnO_2 nanostars) with choline, which is obtained via catalytic hydrolysis of acetylcholine (Ach) by acetylcholinesterase (AChE) (Fig. 7). Due to the fact that various alkaloids restrict AChE activity differently, the presence of distinct alkaloids results in varying degrees of reduction etching of MnO_2, resulting in distinct variations in colorimetric response signals. The detection limits for seven alkaloids have been determined using this sensor array (3.7 nm for berberine, 5.6 nm for berberine chloride, 11.7 nm for jatrorrhizine, 7.0 nm for serine, 25.0 nm for palmatine, 4.8 nm for galanthamine and 5.3 nm for harmane).

The recent study offered a new fluorescent-turn off sensing

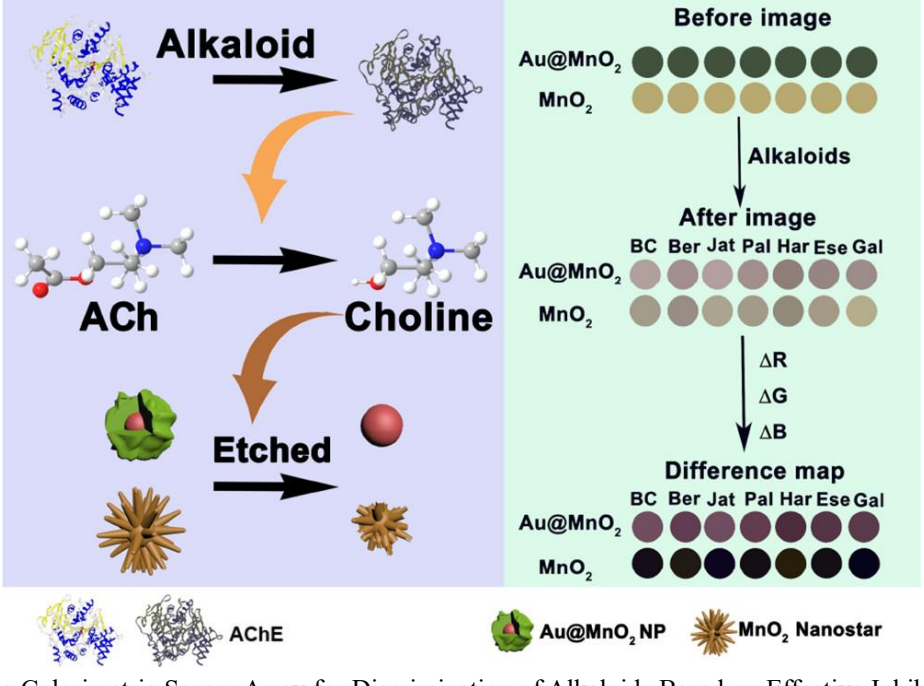

Fig. 7 Schematic of the Colorimetric Sensor Array for Discrimination of Alkaloids Based on Effective Inhibition of AChE and the Etching of Two MnO_2 Nanoparticles. Reproduced with the permission from [53]. Copyright 2021, American Chemical Society.

 © Engineered Science Publisher LLC 2021

label made of Pr(III) doped Gd_2O_3 ($Pr@Gd_2O_3$) nanoparticles (NPs) for detecting 2,4 D in aqueous medium.[54] According to the calculations, $Pr@Gd_2O_3$ NPs are capable of sensing 2,4 D in concentrations ranging from 1 to 25 ppm with a detection limit of 78 ppb under optimal conditions. Additionally, the fabrication of real-time and nondestructive sensor in planta using 1-naphthalene acetic acid (NAA) and 2,4-dichlorophenoxyacetic acid (2,4-D) nanosensors premised on the principle of corona phase molecular recognition (CoPhMoRe). The auxin under investigation has the ability to interact with the cationic polymer through electrostatic interactions via the carboxylate anion over the surface of auxin. The respective CoPhMoRe screen was formed by using the 6 different types of cationic polymer-wrapped inside the single walled nanotube (SWNTs). The binding ability of polymer matrix with the target auxins were studied by titrating the SWNTs against the different concentrations ranging from 1 μM to 5 mM of analytes. The formed sensor has the ability to replace the detrimental and time-consuming conventional state sensing technologies and have higher rate of sensitivity (Fig. 8).[55] By developing an archive of cationic polymers encased across single-walled carbon nanotubes with a diverse affinity for the chemical moieties found on auxins and their derivatives has made it useful for constructing a preferential sensors for artificial auxins with a notably strong quenching response to NAA (46%) and a turn-on response to 2,4-D (51%). The 2,4-D nanosensor established its capabilities for quick assessment of herbicide sensitivity and may aid in elucidating the transport processes of 2,4-D and the basis for herbicide resistance in crops. The herbicide susceptibility testing has further been done by infiltrating the 2,4-D nanosensor. The reference sensors was hydroponically grown pak choi and rice leaves system with supplemented via using hydroponic medium having 1 mm 2,4-D at t = 10 min. A sudden turn on fluorescence response with 64% was observed for pak choi after t = 5h (Fig. 8b). However, there was no change in fluorescence response rice (Fig. 8c). This was mainly explained due to the lack of translocation of 2,4-D in rice during this phase.

Recently, the signal-optimized flower-like silver

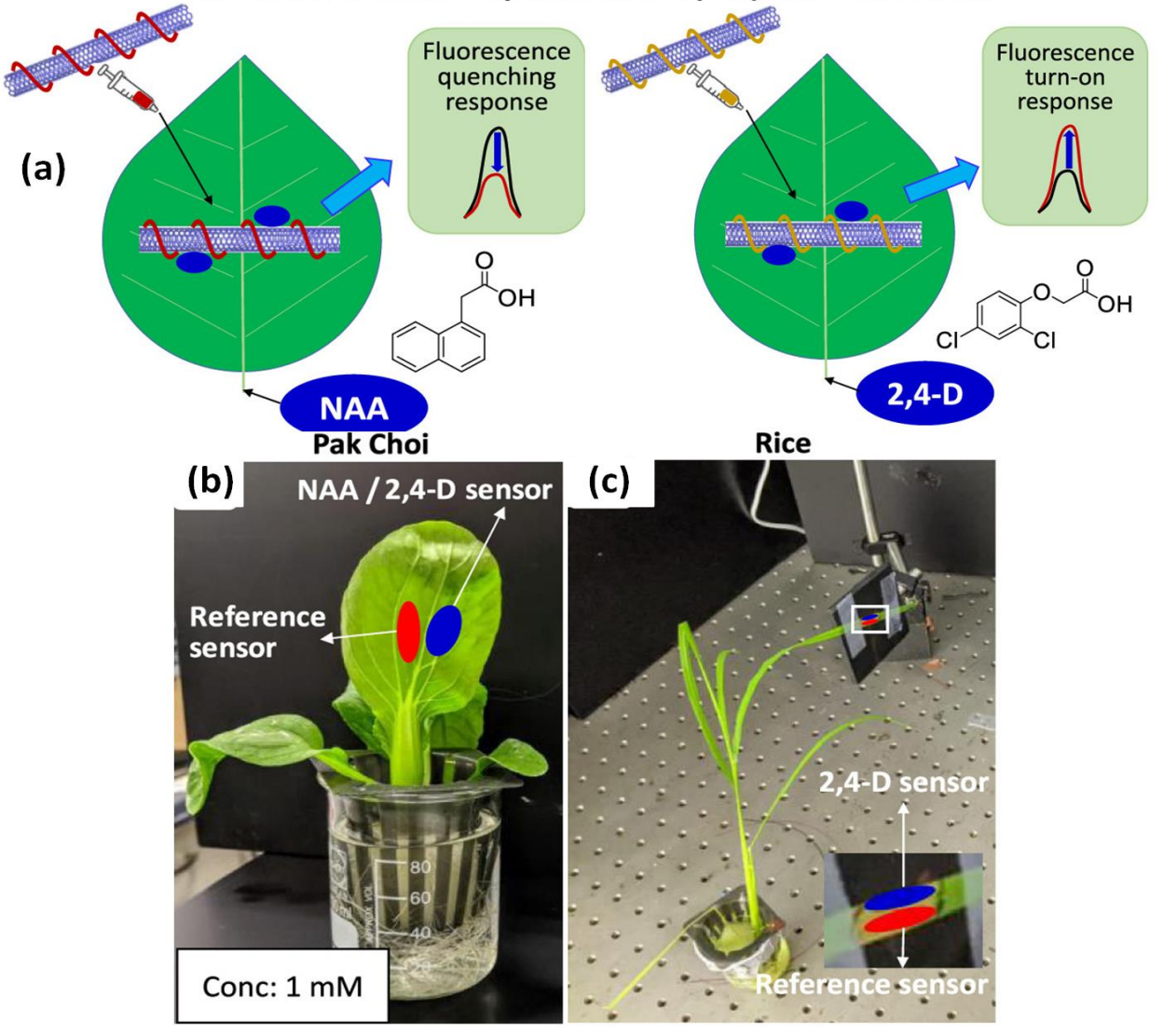

Fig. 8 (a) Schematic representation of in Planta detection of synthetic auxins and the working of sensor in (b) Pak coi and (c) Rice plant respectively. Reproduced with the permission from [55]. Copyright 2021, American Chemical Society.

© Engineered Science Publisher LLC 2021

nanoparticles (AgNP) with an enhancement factor (EF) of 1.39×10^6 at 25 °C is used for pesticide detection in foodstuffs.[56] The fabrication of Ag nanoparticles were done is such a way that a highly rough surface was formed at room temperature conditions. The formation of AgNP involves the pre-nucleation, nucleation, and progression stages during the synthesis. Through solid-phase extraction, the prepared AgNP has been used as a SERS-based sensing platform to detect acetamiprid (AC), methomyl, and 2,4-D residual contents in green tea. During measurements, the presence of Ag nanoparticles has produced strong electromagnetic signals due to the presence of laser excitation. The existence of rough surface has further supported the signal enhancement in presence of target species. The existence of sulfur atom in imidothioate group of methomyl, has further affected the plasmon resonance intensity of AgNP and produced a strong SERS signal during analysis.

Li *et al*. developed a peroxyoxalate chemiluminescence-based nanosensing system for bis (2,4,6-trichlorophenyl) oxalate (TCPO), hydrogen peroxide (H_2O_2). However, the specific-sized gold nanoparticles (Au NPs) have been used for the extremely sensitive, fast, and specific detection of thiram pesticide by using a "on–off" chemiluminescence phenomenon (Fig. 9).[57]

The nanoscale sensing framework generated strong chemiluminescence by chemically excited specific-sized Au NPs. The chemiluminescence property of formed particles was extremely sensitive to thiram and gradually decreased as the discrete energy level of AuNPs changed after interaction with thiram to establish an aggregated structure via intense Au–S bonds. Within a detection time of 40 seconds, the suggested chemiluminescence-based nanosensor could detect thiram with a sensitive and low limit of detection (LOD) of 0.35 nm.

The co-precipitation process was used to generate nanostructured ZnO doped with varied Ce precursor concentrations (1, 5 and 10% mol percent), which were then evaluated for their photocatalytic and chemical sensing properties toward methyl orange (MO) and picric acid (PA) compounds, respectively.[58] Under ultraviolent (UV) illumination, the efficient redox couple of Ce^{3+}/Ce^{4+} reported to enhance the charge separation of Ce-doped ZnO, hence facilitates the release of O_2 and enhancing the catalytic and PA sensing capabilities. Jamil *et al*. developed a Cr_2O_3–TiO_2-modified, compact, and biomimetic nanosensor to address the need for robust and colorimetric hydrogen peroxide sensing platform (Fig. 10).[59] The hydrothermal preparation of Cr_2O_3–TiO_2 nanocomposites was used to create a transducer surface on filter paper using the sol–gel matrix. The hydrogen peroxide added in the presence of Tetramethylbenzidine (TMB). The color of the filter paper sensor changed from green to blue suggesting the existence of hydrogen peroxide. The intensity of the color changed linearly with the concentration of H_2O_2. Red Green Blue (RGB) software has been used to analyze the optical signals as a color analysis model. This paper-based colorimetric platform increased our scientific coefficient of performance by providing a linear range of 0.005–100 μm with a detection limit of 0.003 μm.

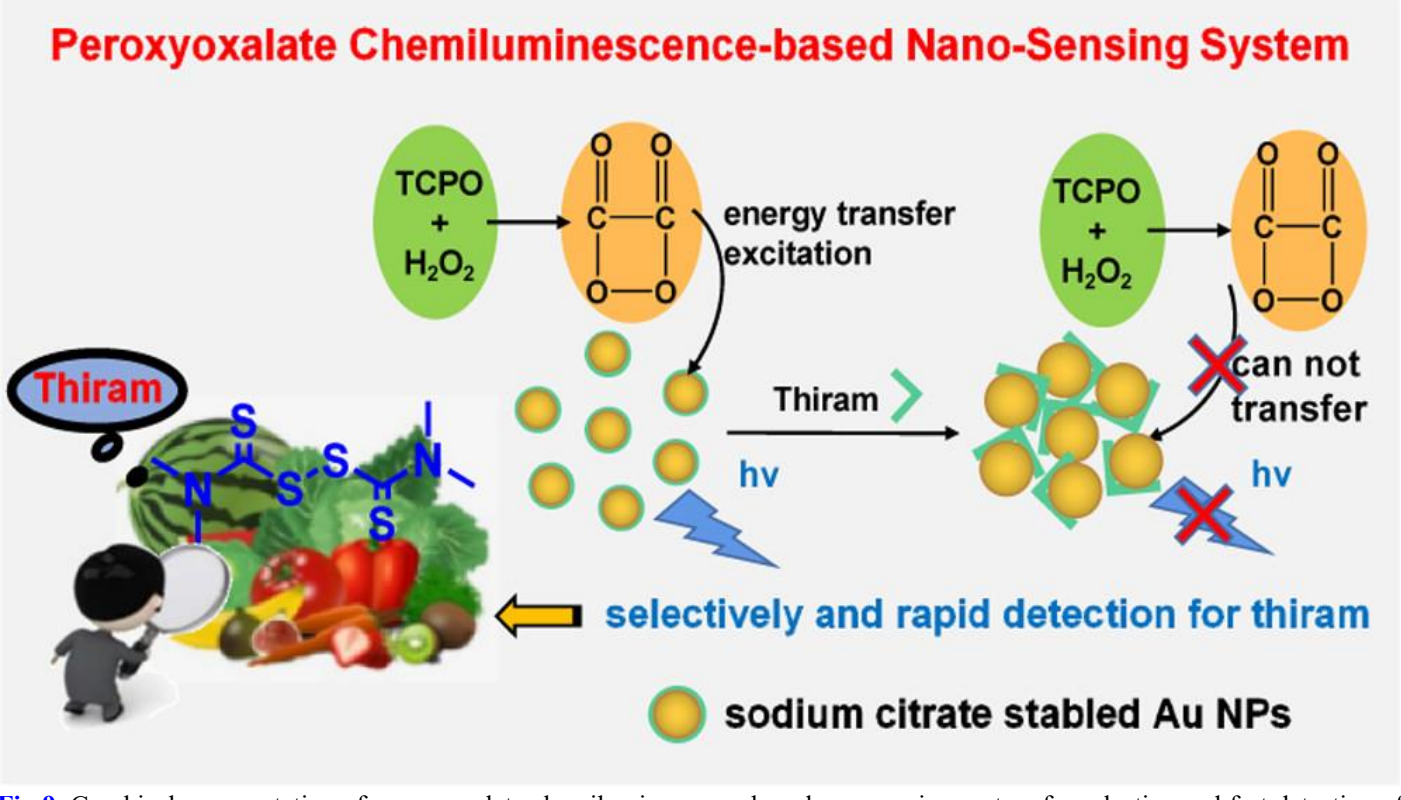

Fig 9. Graphical representation of peroxyoxalate chemiluminescence-based nanosensing system for selective and fast detection of thiram. Reproduced with the permission from [57], Copyright 2021, American Chemical Society.

© Engineered Science Publisher LLC 2021

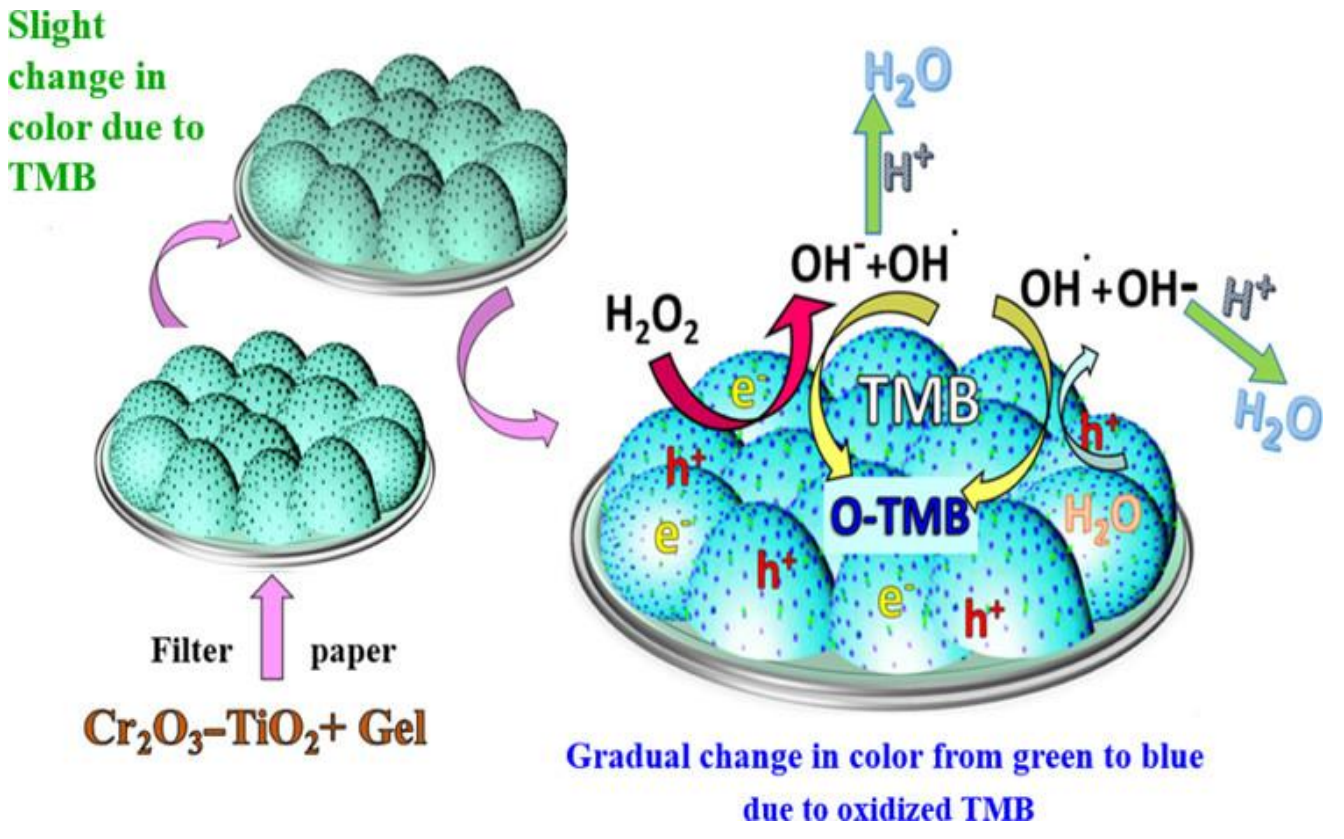

Fig. 10 Conceptual depiction of a biomimetic nanosensor modified with Cr_2O_3 and TiO_2 for colorimetric hydrogen peroxide sensing. Reproduced with the permission from [59], Copyright 2021, American Chemical Society.

A simple one-step chemical approach is shown for the efficient synthesis of Cu_2O, CuO, and $CuNa_2(OH)_4$ crystal structures, as well as the investigation of their electrochemical properties.[60] Under optimal experimental conditions, a linear change in peak current has been obtained for SO_3^{-2} oxidation from 0.2 to 15 mm. Liu developed a simple and environmentally friendly colorimetric sensing analysis technique for effective measurement of melamine. The analysis was based on the redox reaction of gallic acid with Ag^+.[61] They synthesized monodispersed silver nanoparticles (AgNPs) employing gallic acid as a reducing and stabilizing agent. However, when melamine was included in the reaction media, AgNPs starts aggregating. As an outcome, the solution switched color from brilliant yellow to brown, and the color intensity was empirically proportional to the melamine content (Fig. 11). The creation of hydrogen bonds between melamine and gallic acid may be responsible for AgNP aggregation. The developed sensor had an excellent detection limit of 0.099 M (0.012 ppm), which was significantly less than the safety limit. Additionally, the sensing assay exhibited a high degree of selectivity for melamine relative to competing compounds. The interaction of Hg(II) and AuNPs and their influence on DNA adsorption has also been investigated by researchers. Hg(II) stabilized the AuNPs over salt-induced aggregation and enhanced DNA adsorption in the presence of different concentrations up to 1M Hg(II).[62] DNA has been more strongly adsorbed on the AuNPs in the existence of Hg(II).

Liu presented Al–doped $MoSe_2$ (Al–$MoSe_2$) as a potential biosensor for sensing three commonly exhaled volatile organic compounds (VOCs) associated with lung cancer, namely C_5H_8, C_3H_6O and C_3H_4O (Fig. 12). A single Al atom is doped on the Se-vacancy site of the $MoSe_2$ surface, acting as an electron donor and enhancing the electrical conductivity of the system.[63] To gain a complete understanding of the Al–$MoSe_2$ monolayer's, their physicochemical qualities as a sensing material, has been investigated by considering their adsorption and desorption properties, electronic behavior, and thermostability. The results reveal that the Al–$MoSe_2$ monolayer has admirable sensing properties with C_5H_8, C_3H_6O and C_3H_4O at 96.3, 95.6, and 85.7%, respectively. Additionally, the favorable adsorption efficiency and thermostability give the Al–$MoSe_2$ monolayer with high sensitivity and desorbing properties for the recycling detection of three VOCs.

The sensing response (S) for the system has been estimated by measuring the change in the electrical resistance before and after the adsorption of target gas molecules.

The usability of the developed sensor for estimating typical target gas species can be assessed by using the following equation.

$$\sigma = \lambda\ e^{(Bg/2kT)} \quad (12)$$

$$S = (1/\sigma_{gas}\text{-}1/\sigma_{pure})/1/\sigma_{pure} \quad (13)$$

However, σ is defined as the electrical conductivity of the system. λ is constant used during measurement. B_g is defined

© Engineered Science Publisher LLC 2021

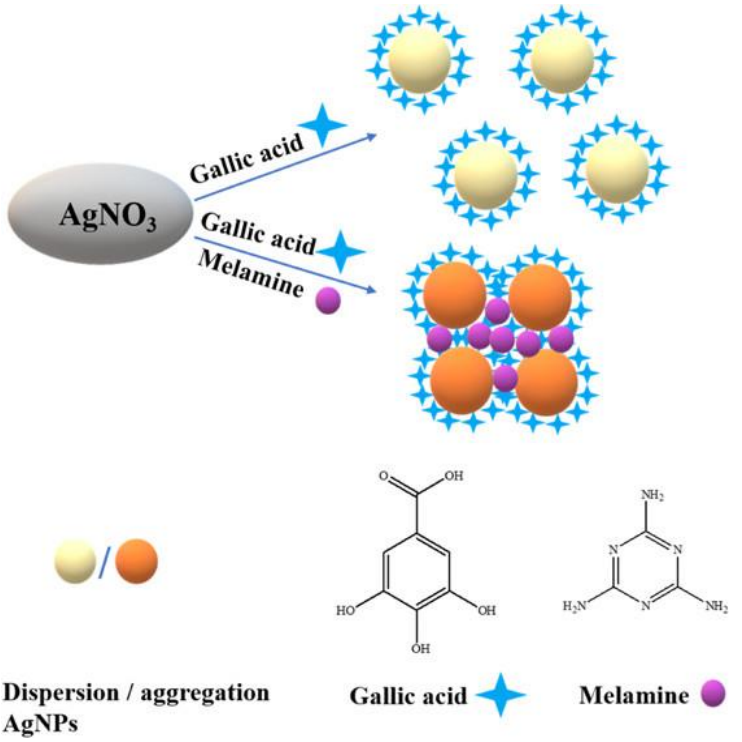

Fig. 11 Representation of methodological strategy for colorimetric sensing of melamine dependent on the redox reaction of gallic acid with Ag^{+}. Reproduced with permission from [61]. Copyright 2021, American Chemical Society.

as the band gap of given system, k is the Boltzmann constant, and T is the working temperature during the measurement. In addition, σ_{gas} and $\sigma_{pure,}$ are defined as the conductivity of the Al−$MoSe_2$ before and after the adsorption of gas molecules. Additionally, the reusability of the sensor was calculated by estimating its recovery property. The recovery time (τ), for the chosen system is calculated by using the following equation.

$$\tau = A^{-1} \cdot e^{(E_a / k_B T)} \quad (14)$$

where, A is defined as the attempted frequency (10^{12} s^{-1}), T is known as the working temperature, and k_B is the Boltzmann constant. E_a is the potential barrier for desorption system.

2.2 Nanomaterials based Sensor for Health diagnosis and checking food quality

An efficient non-enzymatic electrochemical sensor has been fabricated for the detection of lactate.[64] The sensor was built using ZnAl layered double hydroxide (LDH) nanosheets and gold nanoparticles (AuNPs) on boron doped diamond electrodes (BDD). Square wave voltammetry (SWV) studies of lactate binding demonstrated a significant sensitivity of 13.9 A/μm/cm^2 with a broad detection range of 0.1–30 μm, and a low detection limit of 0.1 μm. An attempt has been made to create a biodegradable and accessible non-enzymatic glucose sensor strip based on a laser-scribed graphene electrode (LSGE) doped with gold nanoparticles (AuNPs).[65] The sensor has a linear sensitivity range for glucose levels ranging from 10 μm to 10 mm, having a detection limit of 6.3 μm.

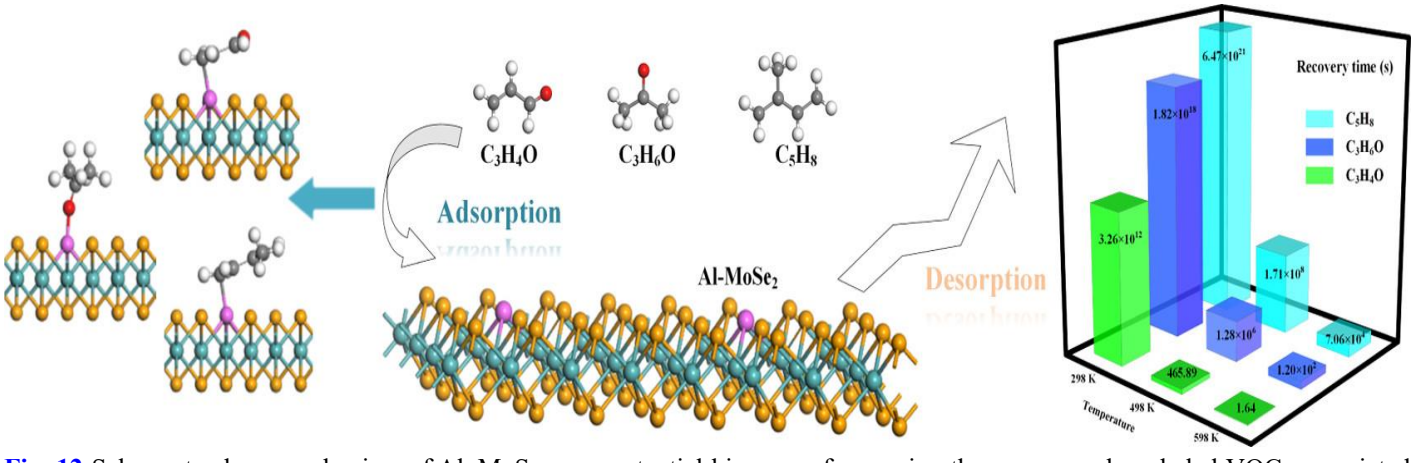

Fig. 12 Scheme to show mechanism of Al–$MoSe_2$ as a potential biosensor for sensing three commonly exhaled VOCs associated with lung cancer, namely C_5H_8, C_3H_6O and C_3H_4O. Reproduced with the permission from [63]. Copyright 2021, American Chemical Society.

 © Engineered Science Publisher LLC 2021

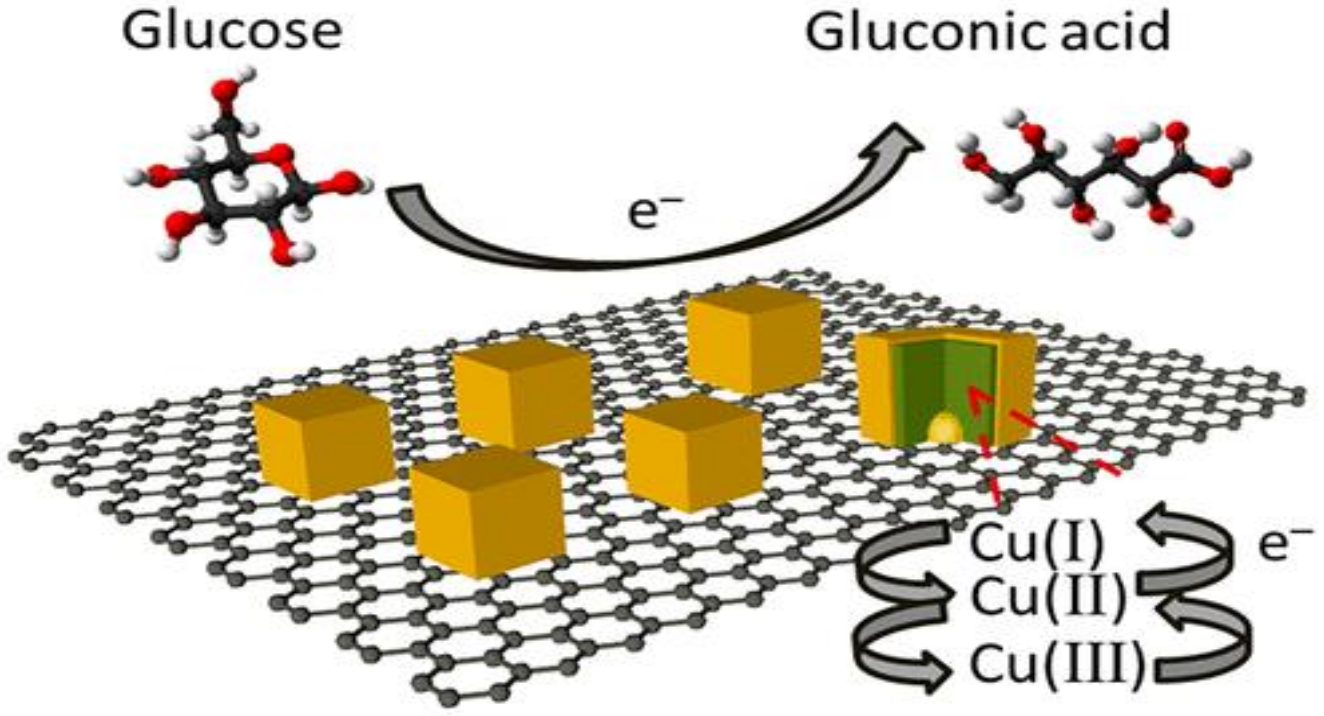

Fig. 13 Illustration of architectural plan for Cu_2O-shell Cu-core nanocubes as an efficient sensor for salivary glucose sensing, Reproduced with permission from [66]. Copyright 2021, American Chemical Society.

Gao and coworkers have constructed a near-homogeneous monolayer of Cu_2O-shell. The band gap values of chosen system made it quite effective for the non-enzymatic sensing of glucose molecules. The electrochemical method has been used for the detection of glucose molecules in the system. Cu-core nanocubes 50 nm in size on a graphene strip substrate using an optimum condition of 1.0 V vs Ag/AgCl, 1 mm [Cu^{2+}], and a deposition duration of 100 s at ambient temperature for glucose sensing (Fig. 13).[66] Cu_2O nanocubes/graphene have been employed to create a high-performance sensor with a detection range of 0.002–17.1 mm and a high accuracy suitable for salivary glucose sensing. It has further been observed that the negative value of the overpotential has the ability to produced smaller sized nanocubes. The formed nanocubes have possessed high number charge density. In addition, the temperature has also affected the deposition rate and the morphology of the formed particles.

For extremely sensitive detection of Phospholipase A2 (PLA2) based on the concept of luminescence resonance energy transfer (LRET) between upconversion nanoparticles (UCNPs) and SYBR Green I (SG) has also gained significant importance.[67] For the analysis, NaYF4:Yb,Tm has been prepared via coating the surface with oleic acid. The LRET efficiency (E) of NaYF4:Yb, Tm has been estimated by using the luminescence lifetimes analysis of donors species by using the following equation:

$$E = 1\text{-}\tau_{DA}/\tau_{D} \quad (15)$$

Here, τ_{DA}, τ_{D} are defined as the luminescence lifetimes of donor in the absence and presence of the acceptor, molecules. The synthesis is carried out by using the modified thermal decomposition process 315 °C under argon gas flow. For checking the presence of Phospholipase A2 (PLA2) in the system, the corresponding inhibitor assay method has been employed by varying the amount from 0 to100 mm. The healthy human plasma samples as well as the affected human being samples with coronary heart disease, pneumonia, and cholelithiasis were also used to study the scope of prepared samples in real practical applications. For forming the sensor, the SYBR Green I (SG) was initially encapsulated inside the close cavity of formed liposome. However, the surface of the NaYF4:Yb,Tm was modified with dsDNA molecules. The emission intensity ratio (I_{522} nm/I_{476} nm) rose continuously with PLA2 quantity in the region of 20 U/L to 400 U/L under suitable circumstances, and the limit of detection (LOD) reached 15 U/L. In this system, the presence of NaYF4:Yb,Tm particles provided an efficient energy donor system. The minimal autofluorescence in these particles has further decreased the background fluorescence during measurement and improved the sensitivity of the sensor.

Chen *et al*. developed an electrochemical sensor using TiO_2 nanoparticles (NPs) for detecting phosphopeptides in protein samples pretreated with AuNPs.[68] The AuNPs can be attached to the polypeptide chain via the amino group at the polypeptide chain's tail when the phosphopeptide solution is prepared with AuNPs (Fig. 14). TiO_2 NPs are precisely linked to the phosphate group on the peptide. The altered AuNPs can enhance the electrode's potential to perceive phosphopeptides electron conduction ability. The formation of the sensor was done by using the Au electrode having diameter of 2 mm. The surface of the gold electrode was thoroughly polished by using

© Engineered Science Publisher LLC 2021

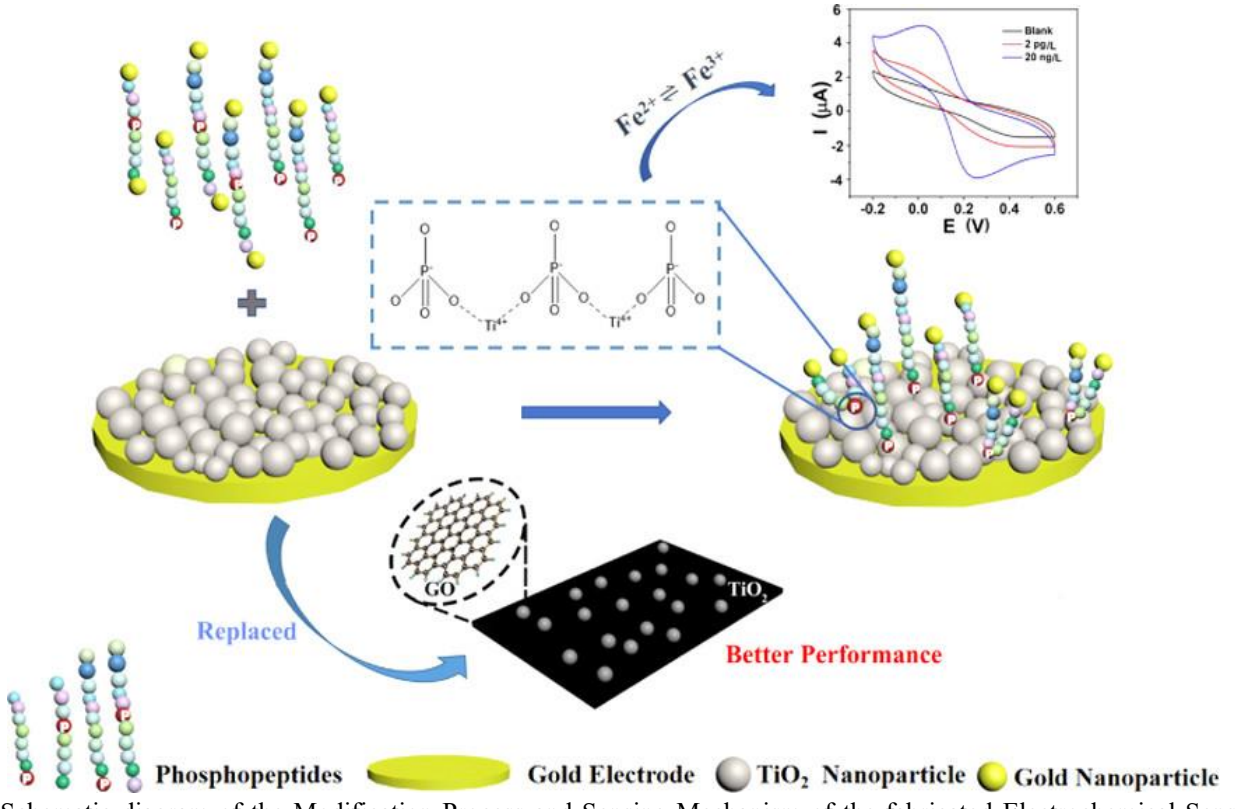

Fig. 14 Schematic diagram of the Modification Process and Sensing Mechanism of the fabricated Electrochemical Sensor [68]. Reproduced with permission from ref. [68]. Copyright 2021, American Chemical Society.

the alumina powder. The cleaning was done by using the deionized water and ethanol. Afterward, the cleaned electrode was voltammetrically cycled in presence of 0.5 M H_2SO_4 having working potential between −0.2 and +1.5 V. Afterwards, around 2 mg of the chosen nanoparticles were dispersed in 490 µL of distilled water and further mixed with 10 µL of 5% Nafion solution. The high binding between TiO_2 and phosphate is mainly used to attach the polypeptide chain over the surface of electrode (Fig. 14). The developed electrochemical sensor exhibited good selectivity, sensitivity and reproducibility, as well as a broad linear concentration range (1 pg/L to 1 mg/L) and a low detection limit (0.24 pg/L) for phosphopeptides. Additionally, they generated TiO_2 and graphene oxide (GO) composite materials to enhance the performance of electrochemical sensors. The results indicate that the electrode modified with an evenly dispersed anatase crystal TiO_2 and GO composite had a lower detection limit (0.37 ag/L).

Behera designed a sensor module using two-dimensional (2D)-MoS_2 nanosheets as the receptor and green fluorescent protein (GFP) as the signal transducer (Fig. 15a).[69] Due to its high surface-to-volume ratio in comparison to other nanomaterials, two-dimensional MoS_2 has been identified as a good option for bioanalyte recognition (Fig. 15b). The modified 2D-MoS_2–GFP conjugates distinguish between 15 diverse proteins at 50 nm with a detection limit of 1mm. The proteins have been successfully differentiated in a binary combination and in the presence of serum (Figs. 15c and 15d). Ten distinct proteins in serum medium at relevant amounts have been correctly categorized with 100% jackknifed accuracy rate, demonstrating the system's potential (Fig. 15e).

An efficient electrochemical sensor for creatinine monitoring was created by altering a carbon paste electrode (CPE) with silver nanoparticles (AgNPs)/multi walled carbon nanotubes (CNTs)/folic acid (FA) system.[70] The electrode demonstrated remarkable selectivity, stability, and a quick response (1.5 s) for creatinine over a concentration range of 1 × 10^{-8} to 2 × 10^{-4} M at pH 7.0, with a detection limit of 0.008 µm. Nitrogen-doped porous carbon antimony (Sb/NPC) nanoparticles are developed in this study for use as a non-enzymatic biosensor.[71] Sb/NPC exhibits redox potential activity and is produced in two steps employing low-cost precursors. The LOD and limit of quantification (LOQ) values for the modified Sb/NPC electrode are 0.74 µm and 2.4 µm, respectively. Singh *et al*. fabricate a novel sensor, using a 3D printed Ag electrode, for detecting blood creatinine (Fig. 16) in the range of 0.01 to 1000 µm (detection limit 10 nm) via an electrochemical chip with a current density ranging from 0.185 to 1.371 mA/cm^2 and has a sensitivity limit of 1.1 µAµm^{-1} cm^{-2} at physiological pH.[72] A series of interference tests demonstrated that analytes such as uric acid, urea, dopamine, and glutathione had no effect on the sensor's performance. Additionally, the sensor response was examined for its ability to accurately detect creatinine in human blood samples in less than a minute. The sensing pathway indicated that the synergistic impact of copper and iron oxide nanoparticles were critical for efficient sensing, with Fe atoms serving as effective sites for creatinine oxidation via the

 © Engineered Science Publisher LLC 2021

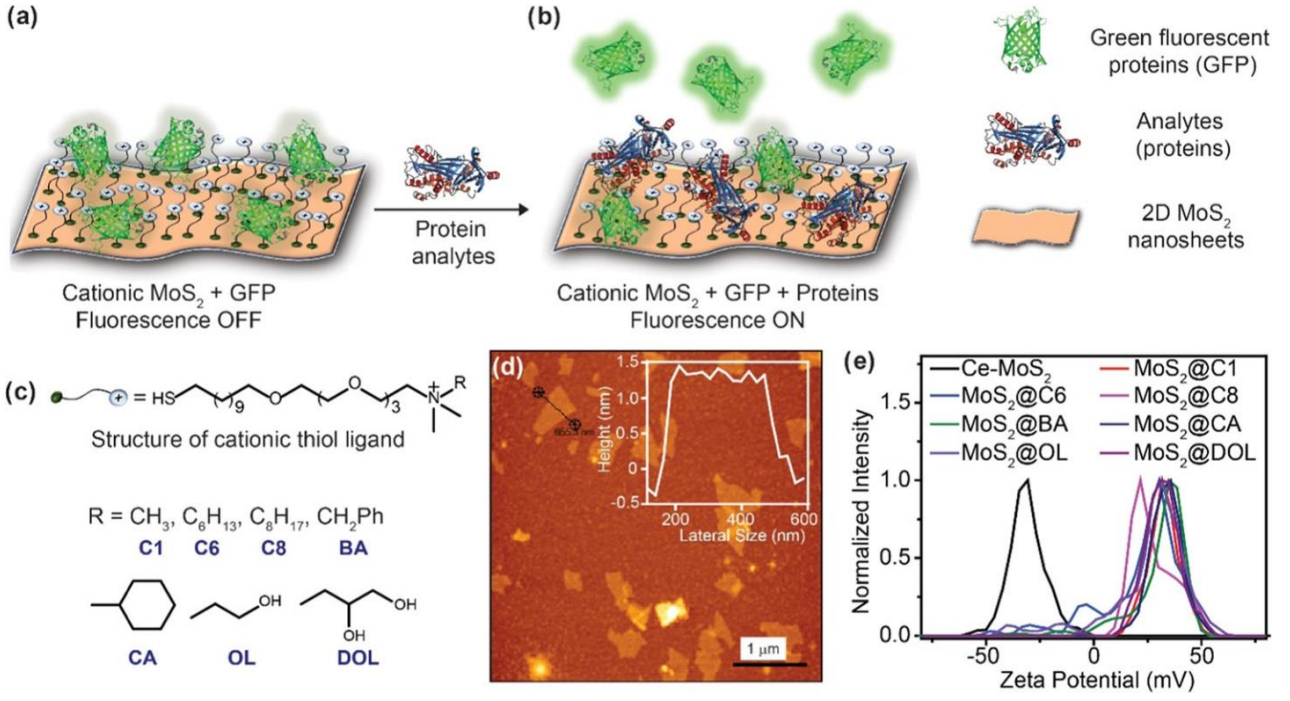

Fig. 15 Schematic representation of sensing systems and characterization of sensor elements. (a) Design of the sensor array: the fluorescence of GFP is quenched by cationic MoS_2 and (b) displacement of GFP from the cationic MoS_2 surface, followed by fluorescence regeneration upon analyte addition. (c) Structure of cationic thiol ligands with different head groups at the non-thiol end. (d) Atomic force microscopy (AFM) image of Ce-MoS_2 with the height profile diagram. (e) ζ-Potential plot for Ce-MoS_2 with and without the thiol ligand functionalization. Reproduced with permission from [69]. Copyright 2021, American Chemical Society.

secondary amine nitrogen and copper nanoparticles serving as an efficient electron mediator via rGO. A new electrochemical sensor based on shock-treated Iron (I) oxide (α-Fe_2O_3) nanoparticles for the rapid identification of Folic acid (FA), Uric acid (UA), and Riboflavin (RF) has also been available in literature.[73] The sensor has been designed to respond precisely over a dynamic range of 0.11 to 691 µm for FA, 0.11 to 722 µm for UA, 0.11 to 624 µm for RF and, with detection limits of 25, 18, and 26 nm, respectively. Du *et al*. used a one-pot hydrothermal approach to carbonise precursors of dried carnation petals and polyethylenimine to create carbon nanodots (CNDs).[74] The produced CNDs exhibit high water solubility, biocompatibility, and photostability making them ideal for use as a dual-responsive nanosensor for measuring vitamin B_2 (VB_2) at different pH range.

Through a strong contact between VB_2 and the surface moieties of CNDs, a novel ratiometric fluorescence resonance energy transfer probe (Fig. 17a) has been established. CNDs emitted at 470 nm, while an increased emission peak at 532 nm was clearly noticed in the presence of VB_2 (Fig. 17b).

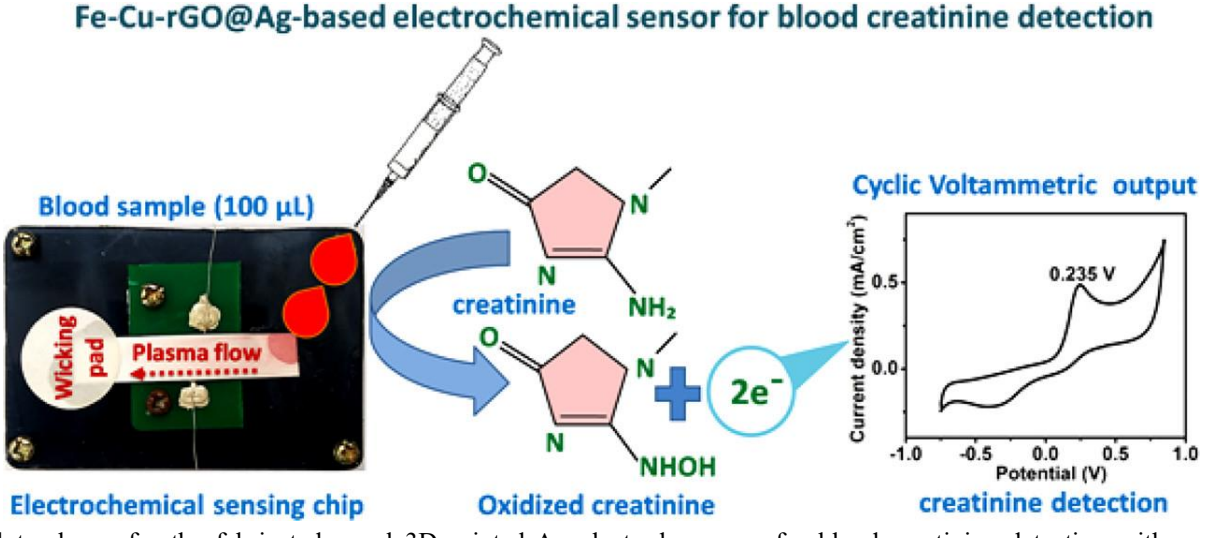

Fig. 16 Pilot scheme for the fabricated novel 3D printed Ag electrode sensor, for blood creatinine detection with respective mechanism of detection and cyclic voltammetric response and Mechanism of Creatinine Oxidation on the Fe−Cu−rGO@Ag Electrode. Reproduced with the permission from [72]. Copyright 2021, American Chemical Society.

© Engineered Science Publisher LLC 2021

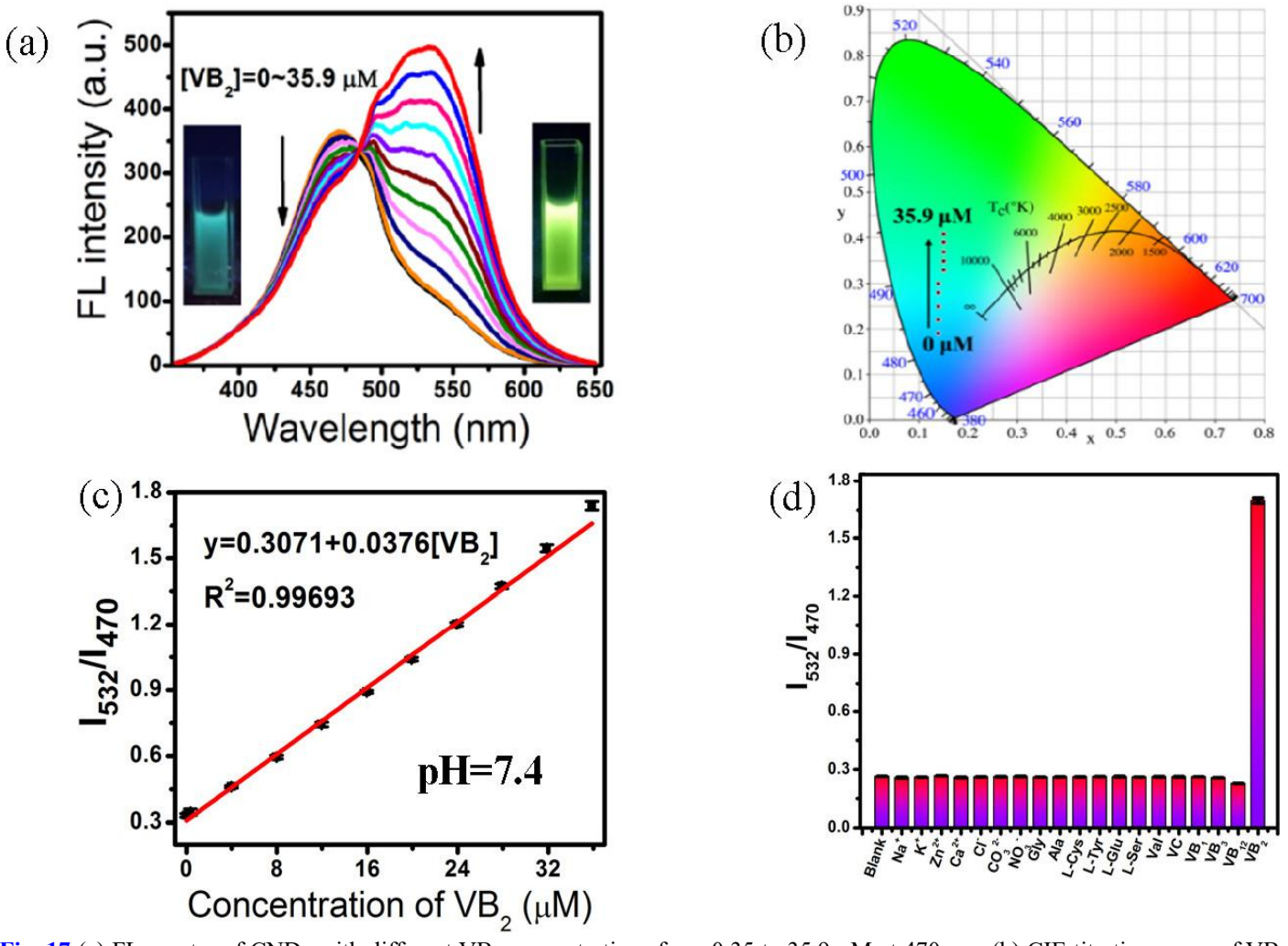

Fig. 17 (a) FL spectra of CNDs with different VB_2 concentrations from 0.35 to 35.9 μM at 470 nm, (b) CIE titration curve of VB_2 from 0.35 to35.9 μM, (c) linear relationship of I_{532}/I_{470} versus different VB_2 concentrations from 0.35 to 35.9 μM at pH 7.4, and (d) FL spectra of selective detection of VB_2. Reproduced with permission from [74], Copyright 2021, American Chemical Society.

I_{532}/I_{470} has a steady response to VB_2 concentrations ranging from 0.35 to 35.9 m with a detection limit of 37.2 nm, and has been successfully employed for VB_2 detection in food and pharmaceutical samples, as well as ratiometric imaging of VB_2 in living cells (Fig. 17c). Additionally, the proposed CNDs exhibited pH-sensitive behavior, suggesting that they might be used as a turn-off fluorescence sensor to monitor pH. The reaction medium pH has further influenced the sensing behavior of the used particles. The presence of excess of hydrogen ions in the reaction medium under acidic conditions has displayed the significant influence over the fluorescence intensity of the system. Therefore, the fluorescence intensity at 470 nm exhibits a strong linear response to pH values ranging from 3.6 to 8, enabling the use of the nanoprobe as a single-emissive probe for intracellular pH detection. However, when the pH of the reaction medium is changed to basic range, the change in intensity is not so effective to observe. The interference studies have also verified the selectivity of the formed sensor towards VB_2 (Fig. 17d).

The development of a versatile colorimetric indicator film based on chitosan (CHI) and broken Riceberry phenolic extract (RPE) have been done successfully.[75] Remarkably, the CHI-RPE film generated a significant colorimetric sensitivity to pH (2–12) variance and volatile ammonia. In response to shrimp spoilage, the CHI-RPE film turned from orange-red to yellow when encased with fresh shrimp. Combining starch nanoparticles (SNPs) with poly(dimethylsiloxane), Wang created an eco-friendly nano-starch-based superhydrophobic coating.[76]

Due to the hierarchical micro and nanostructures generated by SNP aggregates together with the low surface energy of PDMS covering (Fig. 18), the coating displayed superhydrophobic qualities (water contact angle > 152.0° and sliding angle < 9.0°). The high resistance to water, self-cleaning, and decrease of liquid-food residues were validated by using the sensor. After then, an anthocyanin-rich compound was creatively loaded into the SNPs to provide pH responsiveness to the coating. As a result, a waterproof pH-sensing colorimetric coating for food freshness monitoring was successfully produced without the use of a chemical reagent (Fig. 18).

 © Engineered Science Publisher LLC 2021

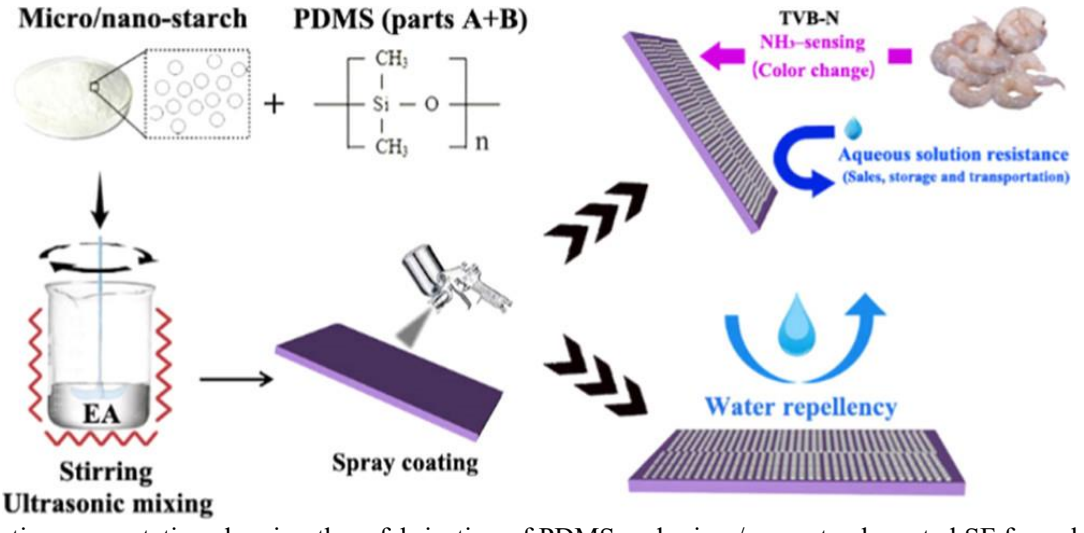

Fig. 18 Schematic representation showing the e fabrication of PDMS and micro/nano-starch coated SF for colorimetric food freshness monitoring. Reproduced with permission from ref. [76]. Copyright 2021, American Chemical Society.

A simple-to-use food packaging indicator with pH and ammonia sensibility has been achieved by introducing betacyanin (5, 10 and 15 mg per g of starch) from paper, flower (Bougainvillea glabra) to a potato starch film produced through the solvent casting method.[77] The film having 15 mg/g betacyanin altered color from bright pink to yellow when the pH was adjusted from 2 to 13. Additionally, it has the capability to detect the presence of ammonia in concentrations ranging between 0.1 and 0.01 mg/L of ammonia in water. Pounds *et al*. has used a glycerol-based nanocomposite core–shell latex film in order to build an adaptable packaging material (Fig. 19) capable of providing high-sensitivity real-time pH measurement of food.[78] To begin, researchers synthesized the pH-responsive dendrimer co-monomer from glycerol and diamine. Then, using a miniemulsion, a nanoencapsulation polymerization method has been used to create core–shell architecture with a customizable nanoshell thickness for a pH-responsive release. Following that, the flexible film enclosed a color-indicative dye that demonstrated extremely sensitive and obvious color changes as the pH of the food decreased and time passed. The use of gold nanoparticles (AuNP)-immersed paper imprinting mass spectrometry imaging (MSI) has been used to monitor pesticide migration activities in a variety of fruits and vegetables.[79] The results indicated that both the octanol-water partition coefficient of pesticides and the water percentage of garden stuffs may have an effect on the discrepancy in pesticide migration into food kernels. Taken together, this nanopaper imprinting MSI has the potential to be a highly effective instrument due to its simplicity, speed, and ease of use, potentially enabling other applications in food analysis. The study proposes the use of monometallic and bimetallic silver and gold nanoparticles to create a colorimetric sensor matrix for the distinction and recognition of triazole fungicides.[80]

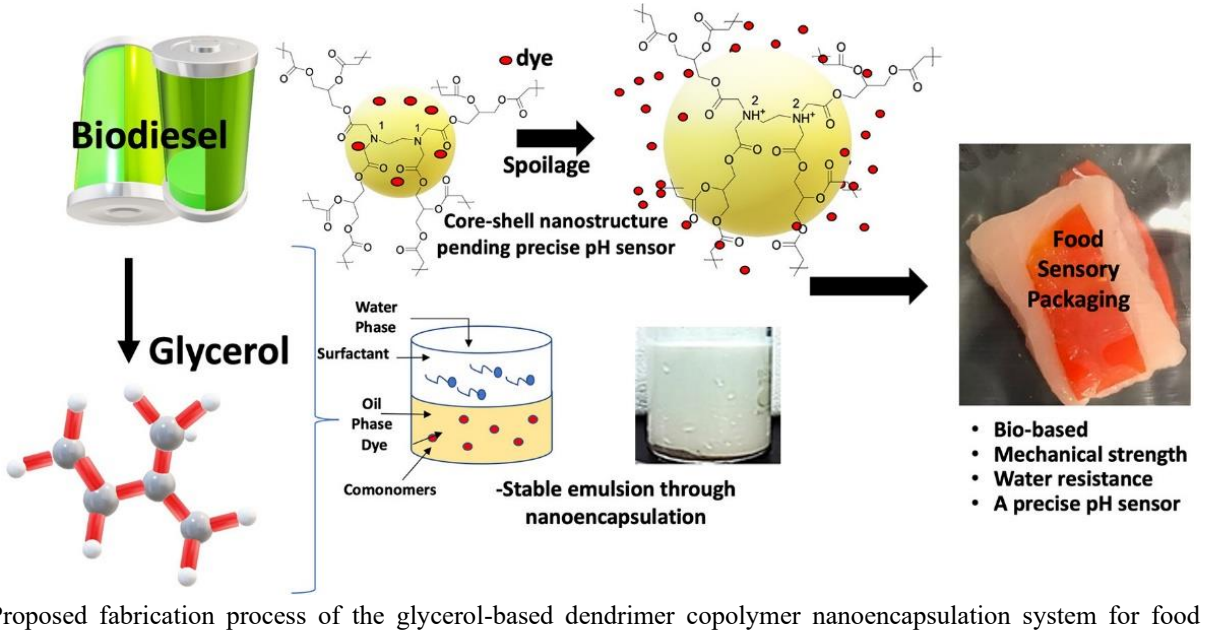

Fig. 19 Proposed fabrication process of the glycerol-based dendrimer copolymer nanoencapsulation system for food spoilage detection. Reproduced with permission from ref. [78]. Copyright 2021, American Chemical Society.

© Engineered Science Publisher LLC 2021

range of 0.1–0.55 g mL^{-1}, pattern recognition approaches such as linear discriminant analysis (LDA) and hierarchical cluster analysis have been used. Ma *et al*. demonstrated the use of a unique noble metal–polymer hybrid film as a SERS substrate for the determination of food fungicides.[81] Due to its transparency and versatility, poly(dimethylsiloxane) (PDMS) film has adopted as a suitable supporting matrix for seed-mediated growth (Fig. 20) of gold nanobushes (Au NBs). In testing 4-nitrothiophenol (4NTP), the as-prepared AuNB–PDMS hybrid film functioned well, with an enhancement factor (EF) of 2.56×10^6. Additionally, the hybrid film's have high sensitivity and elastic qualities which make it a suitable substrate for practical detection. Thus, in situ detection of TBZ, carbaryl, and their mixtures was achieved by utilizing the created hybrid film, which demonstrated a greater sensitivity than the swabbing method. This slightly elevated SERS substrate relying on a transparent and flexible AuNB–PDMS hybrid film offers a wide range of potential applications in the rapid in situ monitoring of biological molecules.

The oxidative polymerization of polythiophene and mixed multi-walled carbon nanotube-graphene (PTH/MWCNT-G) has also been used to develop a robust electrochemical sensor for tartrazine (Tz).[82] Square wave voltammetry (SWV) was used to determine the electrocatalytic activity of the modified electrode, and the results indicated two linear behaviors in the ranges of (1–100 M) and (250–450 M), with a detection limit (LOD) of 0.25 M and 0.303 M, respectively. Tian designed a Fe_3O_4@TiO_2@AuAg SERS substrate with a multifunctional GO coating (Fig. 21a). An external magnetic field induced a relatively uniform substrate attributable to the magnetic core, and electromagnetic advancement from the well-modified Au/Ag binary nanoparticles in combination with the GO's molecular enhancement ability facilitated sensitive SERS-based tracking of trace mixed additives in foods as shown in Fig. 21b.[83] The intrinsic Raman signal of TiO_2 at 149 cm^{-1} was extensively used to serve as a fundamental internal reference for improving the quantitative level of such detection. The multifaceted TiO_2 layer also permitted the efficient green removal of these target compounds within 60 minutes. Remarkable development of a gold nanoparticle-based visual test in conjunction with CRISPR/Cas12a-assisted RT-LAMP, designated as Cas12a-assisted RT-LAMP/AuNP (CLAP) assay, for the quick and sensitive detection of SARS-CoV-2.[84] By naked eye, researchers able to detect SARS-CoV-2 RNA at a concentration of 4 copies/μL in 40 minutes under optimum conditions. CLAP's enhanced specificity is enabled by the sequence-specific recognition property of CRISPR/Cas12a. The obtained SERS spectra versus time for used hybrid substrates under the presence of visible simulator irradiation are shown in Fig. 21b. Lew *et al*. devised a colorimetric serological assay for the detection of SARS-CoV-2 IgGs in patient plasma by conjugating discrete antigenic epitopes to gold nanoparticles (AuNPs).[85] SARS-spike CoV-2's (S) and nucleocapsid (N) proteins contain four immunodominant linear B-cell epitopes that have been identified for their IgG binding affinity and employed as

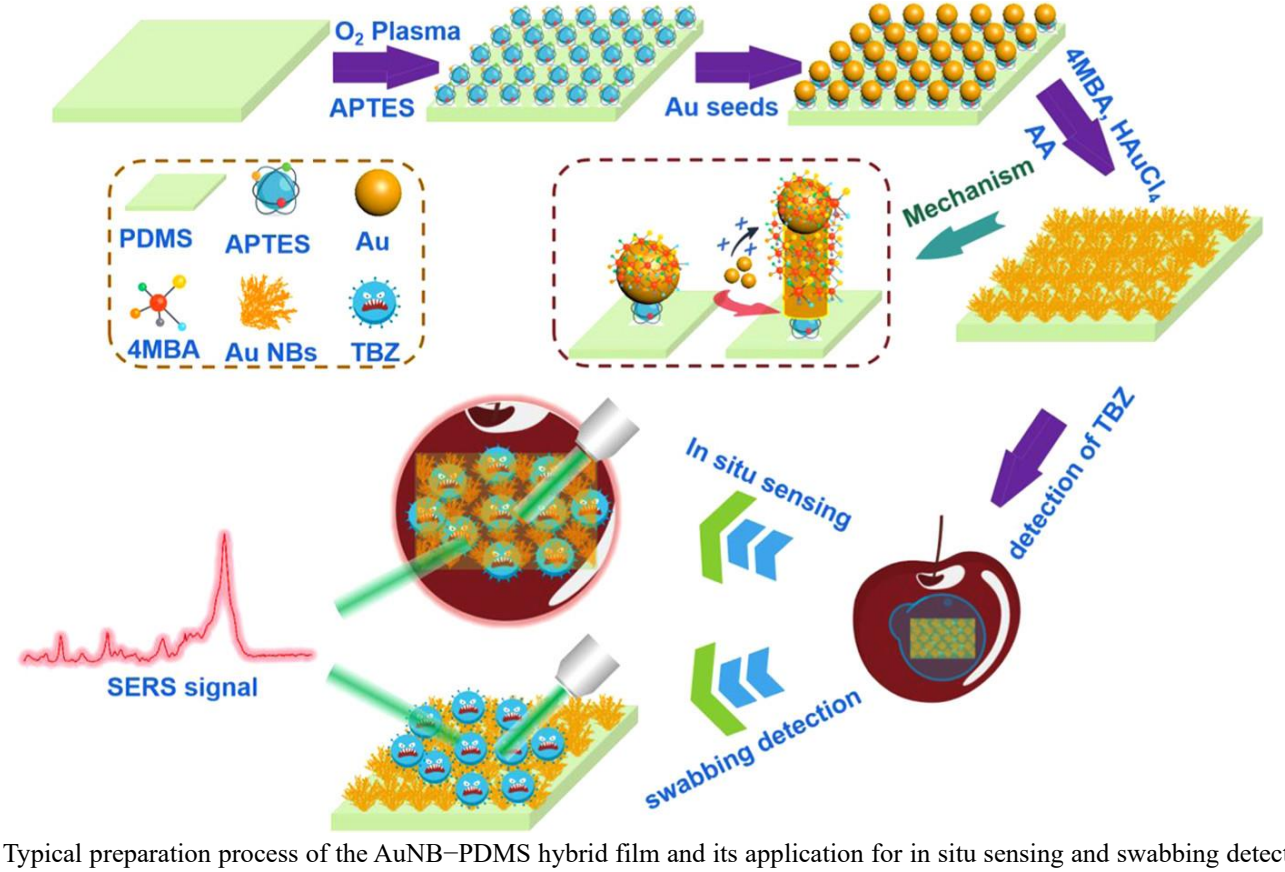

Fig. 20 Typical preparation process of the AuNB−PDMS hybrid film and its application for in situ sensing and swabbing detection of TBZ. Reproduced with permission from [81]. Copyright 2021, American Chemical Society.

 © Engineered Science Publisher LLC 2021

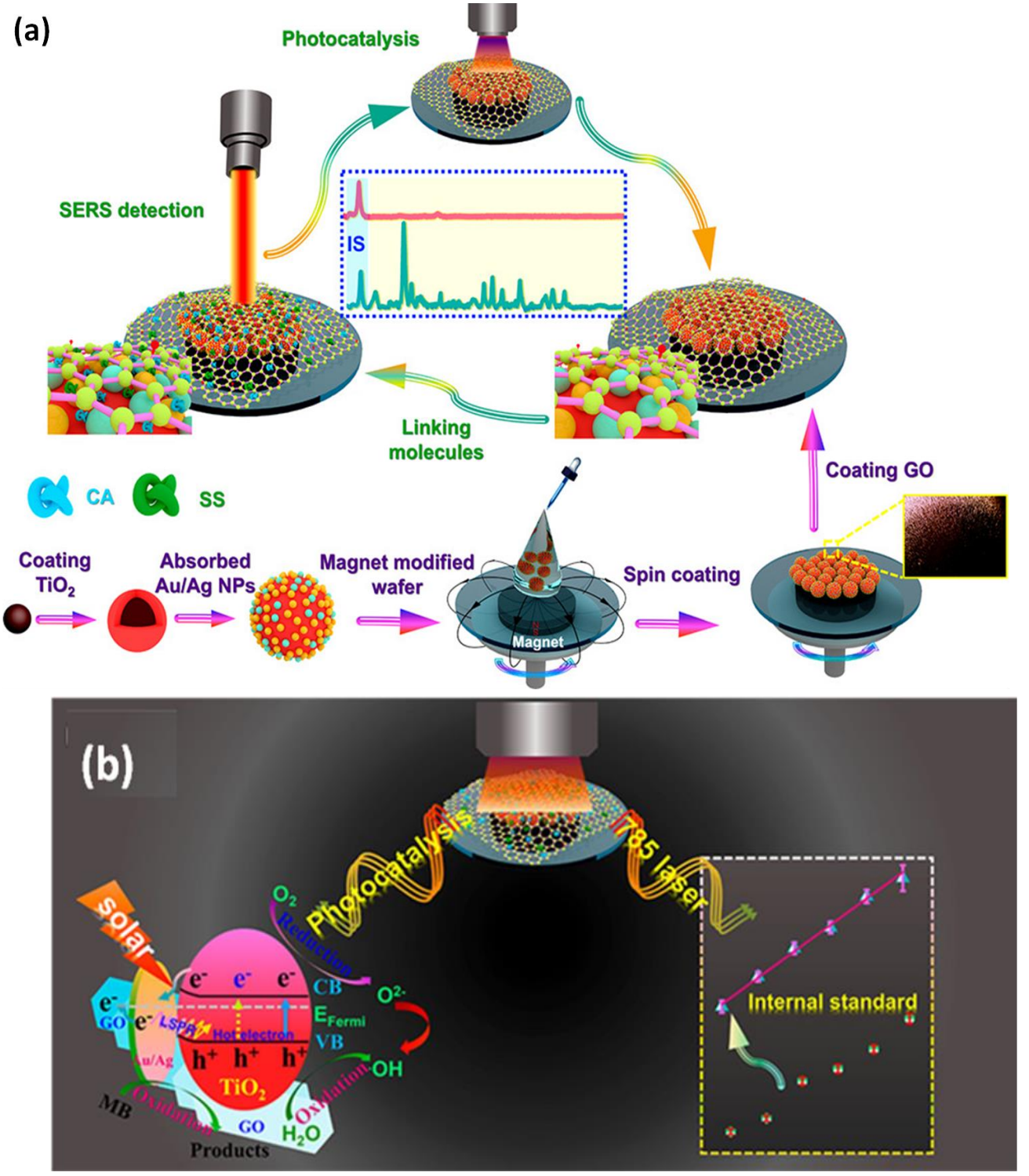

Fig. 21 (a) Schematic representation of fabricated Fe_3O_4@TiO_2@AuAg SERS substrate with multifunctional GO coating and (b) SERS-based signal variations and (c) schematic variations showing the tracking of trace additives in foods [83]. Reproduced with the permission from [83]. Copyright 2021, American Chemical Society.

extremely specific biological motifs on the nanoparticle to detect target antibodies as shown in Fig. 22a. Within 30 minutes of antibody administration, specific bivalent interaction between SARS-CoV-2 antibodies and epitope-functionalized AuNPs causes nanoparticle agglomeration, which exhibits as a distinct optical transition in the AuNPs' plasmon properties. Co-immobilization of two epitopes increased the specificity of the analysis compared to single-epitope AuNPs to 3.2 nM, which is consistent with IgG levels in recovered COVID-19-infected patients (Fig. 22b). When evaluated across 35 clinical plasma samples from patients with varied degrees of sickness severity, the improved nanosensor assay demonstrated 100% accuracy and 83% sensitivity for detecting SARS-CoV-2 infection (Fig. 22c).

© Engineered Science Publisher LLC 2021

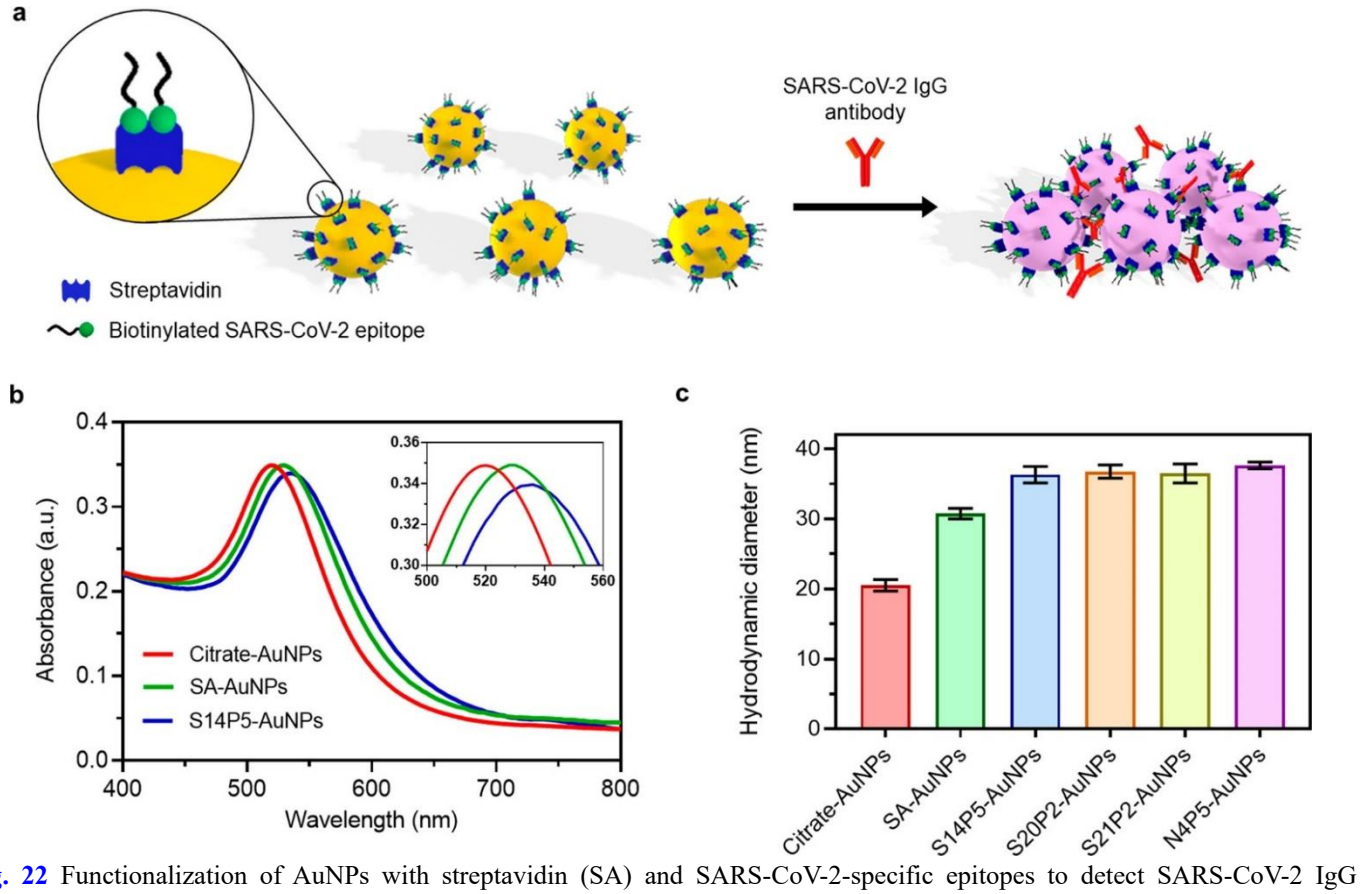

Fig. 22 Functionalization of AuNPs with streptavidin (SA) and SARS-CoV-2-specific epitopes to detect SARS-CoV-2 IgG antibodies. (a) Schematic representation of the nanosensor detection mechanism, which relies on the aggregation of epitope-tagged AuNPs induced by binding to the cognate paratopes of SARS-CoV-2 IgG antibodies. (b) UV−vis spectra of AuNPs upon conjugation of SA and subsequently the biotinylated SARS-CoV-2 epitope peptide S14P5, which was used as a representative epitope. The red-shift in the peak absorbance after consecutive AuNP functionalization with SA and the linear epitope is highlighted in the inset. (c) Hydrodynamic size of AuNPs before and after functionalization with SA and individual linear SARS-CoV-2 epitopes as measured with DLS. Data represent mean ± standard deviation from 3 independent samples. Reproduced with permission from [85]. Copyright 2021, American Chemical Society.

3. Conclusion and future perspective

The development of nanomaterials for sensing applications is still in its infancy, and there is significantly work that need to be done to achieve good commercialized devices. A new generation of sensors with ultra-high sensitivity is still being developed. Due to the wide range of applications, many nanomaterials have not yet been explored in gas/chemical/biological applications. These include new biological sensing applications for emerging contagious diseases and cancer. Additionally, nanomaterials have not been optimized for use in a variety of sensing platforms. Thus, another major area of research is the integration of nanomaterials into innovative sensing platforms, such as plasmonic-based sensors. The application of advanced nanomaterials in sensing application has further enhanced their scope in improving the reactivity of the developed sensor under photo thermal conditions. The improvement in quantum yield and antioxidative properties using advanced nanomaterials has further made them useful in biomedicines. The re-usability of developed sensor and high response rate has further made them quite effective in environmental remediation application.

Additionally, nanomaterial-based sensors should be integrated into automated sample preprocessing and analysis systems such as microfluidics or lab-on-a-chip. At the moment, only a few sensors based on nanomaterials have been successfully integrated in microfluidic systems. One of the most significant issues with nanomaterial-based sensors is their lack of repeatability, which is a result of the difficulty in controlling the structure and layout of the nanomaterial on the sensor. Nanomaterials' highly regulated manufacture and manipulation remain significant technological difficulties. As a result, highly ordered nanomaterials and their application in sensing platforms are among the most exciting areas of nanomaterials research. This results in the emergence of a new field of research known as Nanoarchitectonics, which is a conceptual paradigm for the design and synthesis of dimension-controlled functional nanomaterials. Another major stumbling block is the high cost of mass production due to advanced processing and instrumentation. Thus, another critical area of future research is the development of fabrication processes for low-cost and well-controlled large-

 © Engineered Science Publisher LLC 2021

scale nanostructures in sensing devices.

Acknowledgment
Savita Chaudhary is thankful to DST Inspire Faculty award [IFACH-17], Haryana State Council for Science and Technology [HSCSIT/R&D/2020/476], DST Chandigarh and DST Purse grants II for financial assistance.

Conflict of interest
There are no conflicts to declare.

Supporting information
Not applicable.

References
[1] E. Roduner, *Chem. Soc. Rev.*, 2006, **35**, 583-592, doi: 10.1039/B502142C.
[2] N. Baig, I. Kammakakam, W. Falath, *Adv. Mater.*, 2021, **2**, 1821-1871, doi: 10.1039/D0MA00807A.
[3] R. Roy, A. Tripathi, M. Das, P. D. Dwivedi, *J. Biomed. Nanotech.*, 2011, **7**, 110-111. doi: 10.1166/jbn.2011.1226.
[4] A. Katsumiti, D. Gilliland, I. Arostegui, M. P. Cajaraville, *PloS one*, 2015, **10**, 0129039-0129044, doi: 10.1371/journal.pone.0129039.
[5] A. Puzder, A. Williamson, F. Reboredo, G. Galli, *Phys. Rev. Lett.*, 2003, **91**, 157405-157411, doi: 10.1103/PhysRevLett.91.157405.
[6] P. C. Ray, *Chem. Rev.*, 2010, **110**, 5332-5365, doi: 10.1021/cr900335q.
[7] V. Stone, B. Nowack, A. Baun, N. van den Brink, F. von der Kammer, M. Dusinska, R. Handy, S. Hankin, M. Hassellöv, E. Joner, *Sci. Total Environ.*, 2010, **408**, 1745-1754, doi: 10.1016/j.scitotenv.2009.10.035.
[8] W. Wohlleben, *J. Nanoparticle Res.*, 2012, **14**, 1-18, doi: 10.1007/s11051-012-1300-z.
[9] S. Ray, Y. V. Kolen'ko, D. Fu, R. Gallage, N. Sakamoto, T. Watanabe, M. Yoshimura, M. Itoh, *Small*, 2006, **2**, 1427-1431, doi: 10.1002/smll.200600297.
[10] B. Su, C. Zhang, S. Chen, X. Zhang, L. Chen, Y. Wu, Y. Nie, X. Kan, Y. Song, L. Jiang, *Adv. Mater.*, 2014, **26**, 2501-2507, doi: 10.1002/adma.201305249.
[11] C. E. Boott, J. Gwyther, R. L. Harniman, D. W. Hayward, I. Manners, *Nat. Chem.*, 2017, **9**, 785-792, doi: 10.1038/nchem.2721.
[12] W. C. Hu, M. R. Younis, Y. Zhou, C. Wang, X. H. Xia, *Small*, 2020, **16**, 2000553-2000562, doi: 10.1002/smll.202000553.
[13] M. Guo, P. Liu, B. Huang, Y. Qiu, Y. Wei, Y. Ma, *Appl. Surf. Sci.*, 2019, **476**, 1072-1078, doi: 10.1016/j.apsusc.2019.01.235.
[14] Q. Zhang, M. Li, B. Luo, Y. Luo, H. Jiang, C. Chen, S. Wang, D. Min, *J. Hazard. Mater.*, 2021, **402**, 123445-123452, doi: 10.1016/j.jhazmat.2020.123445.
[15] Z. Zheng, H.-H. Wu, H. Liu, Q. Zhang, X. He, S. Yu, V. Petrova, J. Feng, R. Kostecki, P. Liu, *ACS Nano*, 2020, **14**, 9545-9561, doi: 10.1021/acsnano.9b08575.
[16] L. Zeng, L. Xiao, J. Zhang, H. Fu, *J. Nanosci. Nanotechnol.*, 2020, **20**, 4607-4618, doi: 10.1166/jnn.2020.18491.
[17] O. V. Salata, *J. Nanobiotechnology*, 2004, **2**, 1-6, doi: 10.1186/1477-3155-2-3.
[18] L. Yu, Z. Song, J. Peng, M. Yang, H. Zhi, H. He, *Trends Anal. Chem.*, 2020, **127**, 115880-115887, doi: 10.1016/j.trac.2020.115880.
[19] S. Samsami, M. Mohamadizaniani, M. H. Sarrafzadeh, E. R. Rene, M. Firoozbahr, *Process Saf. Environ. Prot.*, 2020, **143**, 138-163, doi: 10.1016/j.psep.2020.05.034.
[20] N. Rabiee, M. Bagherzadeh, M. Kiani, A. M. Ghadiri, F. Etessamifar, A. H. Jaberizadeh, A. Shakeri, *Int. J. Nanomed.*, 2020, **15**, 3983-3989, doi: 10.2147/IJN.S255398.
[21] A. H. Kianfar, M. A. Arayesh, *J. Environ. Chem. Eng.*, 2020, **8**, 103640-103648, doi: 10.1016/j.jece.2019.103640.
[22] R. Nißler, O. Bader, M. Dohmen, S. G. Walter, C. Noll, G. Selvaggio, U. Groß, S. Kruss, *Nat. Commun.*, 2020, **11**, 1-12, doi: 10.1038/s41467-020-19718-5.
[23] D. Zhang, L. Peng, X. Shang, W. Zheng, H. You, T. Xu, B. Ma, B. Ren, J. Fang, *Nat. Commun.*, 2020, **11**, 1-7, doi: 10.1038/s41467-020-16329-y.
[24] R. Sha, T. K. Bhattacharyya, *Electrochim. Acta*, 2020, **349**, 136370-136378, doi: 10.1016/j.electacta.2020.136370.
[25] P. Sharma, V. Pandey, M. M. M. Sharma, A. Patra, B. Singh, S. Mehta, A. Husen, *Nanoscale Res. Lett.*, 2021, **16**, 1-24, doi: 10.1186/s11671-021-03593-0.
[26] H. Pu, Y. Xu, D. W. Sun, Q. Wei, X. Li, *Crit. Rev. Food Sci. Nutr.*, 2021, **61**, 2107-2124, doi: 10.1080/10408398.2020.1808877.
[27] K.H. Sun, W. C. Chien, H. F. Hsu, *Nanoscale Res. Lett.*, 2021, **16**, 1-8, doi: 10.1186/s11671-021-03539-6.
[28] X. Yu, M. Kilani, A. Siddiqui, G. Mao, *Adv. Mater. Technol.*, 2020, **5**, 2000554, doi: 10.1002/admt.202000554.
[29] M. Liu, K. Cheng, X. Qin, Z. Wei, Y. Peng, P. Li, P. Liu, N. Cao, J. Huang, Y. Feng, *IEEE Trans Nanotechnol.*, 2021, **20**, 229-233, doi: 10.1109/TNANO.2021.3064380.
[30] T. Yang, T. V. Duncan, *Nat. Nanotechnol.*, 2021, **16**, 251-265, doi: 10.1038/s41565-021-00867-7,
[31] T. S. Munonde, P. N. Nomngongo, *Sensors*, 2021, **21**, 131-138, doi: 10.3390/s21010131.
[32] M. Tonezzer, *Chemosensors*, 2021, **9**, 2-9, doi: 10.3390/chemosensors9010002.

© Engineered Science Publisher LLC 2021

[33] A. dos Santos, F. Sabino, A. Rovisco, P. Barquinha, H. Águas, E. Fortunato, R. Martins, R. Igreja, *Chemosensors*, 2021, **9**, 27-33, doi: 10.3390/chemosensors9020027.
[34] Y. Xu, L. Zheng, C. Yang, W. Zheng, X. Liu, J. Zhang, *Sens. Actuator B-Chem.*, 2020, **310**, 127846-127852, doi: 10.1016/j.snb.2020.127846.
[35] D. Hu, L. Yang, S. Deng, Y. Hao, K. Zhang, X. Wang, Y. Liu, H. Liu, Y. Chen, M. Xie, *Sens. Actuator B-Chem.*, 2021, **334**, 129653, doi: 10.1016/j.snb.2021.129653.
[36] S. Bilge, B. Dogan-Topal, E. B. Atici, A. Sınağ, S. A. Ozkan, *Sens. Actuator B-Chem.*, 2021, **343**, 130109, doi: 10.1016/j.snb.2021.130109.
[37] H. Shi, S. Yan, X. Yang, X. Wu, W. Wu, E. Hua, *Micromachines*, 2021, **12**, 495, doi: 10.3390/mi12050495.
[38] X. Zhu, P. Liu, T. Xue, Y. Ge, S. Ai, Y. Sheng, R. Wu, L. Xu, K. Tang, Y. Wen, *Ceram. Int.*, 2021, **47**, 173-184, doi: 10.1016/j.ceramint.2020.08.121.
[39] H. A. Hussein, R. M. El Nashar, I. M. El-Sherbiny, R. Y. Hassan, *Biosens. Bioelectron.*, 2021, **191**, 113435, doi: 10.1016/j.bios.2021.113435.
[40] Y. Navale, S. Navale, M. Chougule, N. Ramgir, V. Patil, *J. Mater. Sci.: Mater. Electron.*, 2021, **1**, 1-14, doi: 10.1007/s10854-021-06360-0.
[41] Y. Song, Y. Xu, Q. Guo, Z. Hua, F. Yin, W. Yuan, *ACS Appl. Mater. Interfaces*, 2021, **1**, 1-7, doi: 10.1021/acsami.1c12154.
[42] J. G. Thangamani, S. K. Pasha, *Chemosphere*, 2021, **277**, 130237, doi: 10.1016/j.chemosphere.2021.130237.
[43] D. Feng, L. Du, X. Xing, C. Wang, J. Chen, Z. Zhu, Y. Tian, D. Yang, *ACS Sens.*, 2021, **6**, 733-741, doi: 10.1021/acssensors.0c01280.
[44] S. Jaballah, H. Dahman, G. Neri, L. El Mir, *J. Inorg. Organomet. Polym. Mater.*, 2021, **31**, 1653-1667, doi: 10.1007/s10904-020-01796-z.
[45] G. Xu, F. Wei, Y. Cen, X. Cheng, Q. Hu, *ACS Biomater. Sci. Eng.*, 2020, **6**, 6086-6094, doi: 10.1021/acsbiomaterials.0c00842.
[46] L. Zhou, Z. Hu, H. Y. Li, J. Liu, Y. Zeng, J. Wang, Y. Huang, L. Miao, G. Zhang, Y. Huang, *ACS Appl. Mater. Interfaces*, 2021, **13**, 25111–25120, doi: 10.1021/acsami.1c04651.
[47] N. A. Pandit, M. Shahazad, T. Ahmad, *Mater. Today: Proc.*, 2021, **36**, 724-729, doi: 10.1016/j.matpr.2020.04.769.
[48] J. Y. Jeon, S. J. Park, T. J. Ha, *ACS Appl. Mater. Interfaces*, 2021, **13**, 25082–25091 doi: 10.1021/acsami.1c03283.
[49] M. C. Stoian, I. Mihalache, M. Matache, A. Radoi, *Dyes Pigm.*, 2021, **187**, 109144, doi: 10.1016/j.dyepig.2021.109144.
[50] A. De, A. Kumari, P. Jain, A. K. Manna, G. Bhattacharjee, *Inorg. Nano-Met. Chem.*, 2021, **51**, 1214-1225, doi: 10.1080/24701556.2020.1826523.
[51] Q. Y. Liu, Z. Q. Bu, Q. F. Yao, X. Ding, L. Q. Xia, W. T. Huang, *ACS Appl. Nano Mater.*, 2021, **4**, 7086-7096, doi: 10.1021/acsanm.1c01102.
[52] M. Kumar, K. Negi, A. Umar, M. Chauhan, *Chem. pap.*, 2021, **75**, 1555-1566, doi: 10.1007/s11696-020-01388-8.
[53] Y. Li, Z. Qian, C. Shen, Z. Gao, K. Tang, Z. Liu, Z. Chen, *ACS Appl. Nano Mater.*, 2021, **4**, 8465-8472, doi: 10.1021/acsanm.1c01741.
[54] S. Kumar, D. Mehta, S. Chaudhary, G. R. Chaudhary, *J. Mol. Liq.*, 2021, **324**, 114712-114720, doi: 10.1016/j.molliq.2020.114712.
[55] M. C. Y. Ang, N. Dhar, D. T. Khong, T. T. S. Lew, M. Park, S. Sarangapani, J. Cui, A. Dehadrai, G. P. Singh, M. B. Chan-Park, *ACS Sens.*, 2021, **6**, 3032–3046, doi: 10.1021/acssensors.1c01022.
[56] M. M. Hassan, M. Zareef, T. Jiao, S. Liu, Y. Xu, A. Viswadevarayalu, H. Li, Q. Chen, *Food Chem.*, 2021, **338**, 127796-127805, doi: 10.1016/j.foodchem.2020.127796.
[57] L. Li, D. Lin, F. Yang, Y. Xiao, L. Yang, S. Yu, C. Jiang, *ACS Appl. Nano Mater.*, 2021, **4**, 3932-3939, doi: 10.1021/acsanm.1c00305.
[58] M. Kumar, M. S. Chauhan, M. S. Akhtar, A. Umar, *Ceram. Int.*, 2021, **47**, 3089-3098, doi: 10.1016/j.ceramint.2020.09.145.
[59] S. Jamil, M. Nasir, Y. Ali, S. Nadeem, S. Rashid, M. Y. Javed, A. Hayat, *ACS Omega*, 2021, **6**, 23368–23377 doi: 10.1021/acsomega.1c03119.
[60] V. Sudha, G. Murugadoss, R. Thangamuthu, *Sci. Rep.*, 2021, **11**, 1-12, doi: 10.1038/s41598-021-82741-z.
[61] X. Liu, J. Wang, Y. Wang, C. Huang, Z. Wang, L. Liu, *ACS Omega*, 2021, **6**, 23630–23635 doi: 10.1021/acsomega.1c03927.
[62] Y. Hu, Z. Huang, B. Liu, J. Liu, *ACS Appl. Nano Mater.*, 2021, **4**, 1377-1384, doi: 10.1021/acsanm.0c02923.
[63] T. Liu, Z. Cui, X. Li, H. Cui, Y. Liu, *ACS Omega*, 2020, **6**, 988-995, doi: 10.1021/acsomega.0c05654.
[64] M. A. Djebbi, S. Boubakri, M. Braiek, N. Jaffrezic-Renault, P. Namour, A. B. H. Amara, *J. Electrochem. Soc.*, 2021, **168**, 057529-057536, doi: 10.1149/1945-7111/ac0226/meta.
[65] B. Zhu, L. Yu, S. Beikzadeh, S. Zhang, P. Zhang, L. Wang, J. Travas-Sejdic, *Electrochim. Acta*, 2021, **378**, 138132-138142, doi: 10.1016/j.electacta.2021.138132.
[66] W. Gao, X. Zhou, N. F. Heinig, J. P. Thomas, L. Zhang, K. T. Leung, *ACS Appl. Nano Mater.*, 2021, **4**, 4790–4799, doi: 10.1021/acsanm.1c00381.

© Engineered Science Publisher LLC 2021

[67] D. Luo, C. Zhang, Y. Fang, Y. Shen, Y. Liang, Y. Xia, F. Wu, X. Chen, J. Liu, J. Chen, *Anal. Chim. Acta*, 2021, **1143**, 37-44, doi: 10.1016/j.aca.2020.11.025.
[68] Y. Chen, B. Liu, Z. Chen, X. Zuo, *Anal. Chem.*, 2021, **93**, 10635-10643, doi: 10.1021/acs.analchem.1c01973.
[69] P. Behera, K. K. Singh, S. Pandit, D. Saha, D. K. Saini, M. De, *ACS Appl. Nano Mater.*, 2021, **4**, 3843-3851, doi: 10.1021/acsanm.1c00244.
[70] A. Fekry, S. Abdel-Gawad, R. Tammam, M. Zayed, *Measurement*, 2020, **163**, 107958, doi: 10.1016/j.measurement.2020.107958.
[71] M. Jamil, B. Fatima, D. Hussain, T. A. Chohan, S. Majeed, M. Imran, A. A. Khan, S. Manzoor, R. Nawaz, M. N. Ashiq, *Bioelectrochemistry*, 2021, **140**, 107815, doi: 10.1016/j.bioelechem.2021.107815.
[72] P. Singh, S. Mandal, D. Roy, N. Chanda, *ACS Biomater. Sci. Eng.*, 2021, **7**, 3446–3458, doi: 10.1021/acsbiomaterials.1c00484.
[73] S. Meenakshi, S. Anitta, A. Sivakumar, S. M. B. Dhas, C. Sekar, *Microchem. J.*, 2021, **168**, 106403, doi: 10.1016/j.microc.2021.106403.
[74] F. Du, Z. Cheng, G. Wang, M. Li, W. Lu, S. Shuang, C. Dong, *J. Agric. Food Chem.*, 2021, **69**, 2836-2844, doi: 10.1021/acs.jafc.0c07019.
[75] F. N. Eze, T. J. Jayeoye, S. Singh, *Food Chem.*, 2022, **366**, 130574, doi: 10.1016/j.foodchem.2021.130574.
[76] F. Wang, L. Qiu, Y. Tian, *Biomacromolecules*, 2021, **9**, 3769–3779, doi: 10.1021/acs.biomac.1c00588.
[77] S. Naghdi, M. Rezaei, M. Abdollahi, *Int. J. Biol. Macromol.*, 2021, **191**, 161-170, doi: 10.1016/j.ijbiomac.2021.09.045.
[78] K. Pounds, S. Jairam, H. Bao, S. Meng, L. Zhang, S. Godinez, D. A. Savin, W. Pelletier, M. J. Correll, Z. Tong, *ACS Appl. Mater. Interfaces*, 2021, **13**, 23268-23281, doi: 10.1021/acsami.1c05145.
[79] R. Qin, P. Li, M. Du, L. Ma, Y. Huang, Z. Yin, Y. Zhang, D. Chen, H. Xu, X. Wu, *Nanomaterials*, 2021, **11**, 1327, doi: 10.3390/nano11051327.
[80] K. Kalantari, N. Fahimi-Kashani, M. R. Hormozi-Nezhada, *Anal. Bioanal. Chem.*, 2021, **1**, 1-12, doi: 10.1007/s00216-021-03272-0.
[81] Y. Ma, Y. Chen, Y. Tian, C. Gu, T. Jiang, *J. Agric. Food Chem.*, 2021, **69**, 1975-1983, doi: 10.1021/acs.jafc.0c06562.
[82] H. H. AL-Refai, A. A. Ganash, M. A. Hussein, *Synth. Met.*, 2021, **280**, 116875, doi: 10.1016/j.synthmet.2021.116875.
[83] Y. Tian, H. Liu, Y. Chen, C. Gu, G. Wei, T. Jiang, *ACS Sustain. Chem. Eng.*, 2020, **8**, 16990-16999, doi: 10.1021/acssuschemeng.0c07447.
[84] Y. Zhang, M. Chen, C. Liu, J. Chen, X. Luo, Y. Xue, Q. Liang, L. Zhou, Y. Tao, M. Li, *Sens. Actuators B Chem.*, 2021, **345**, 130411, doi: 10.1016/j.snb.2021.130411.
[85] T. T. S. Lew, K. M. M. Aung, S. Y. Ow, S. N. Amrun, L. Sutarlie, L. F. Ng, X. Su, *ACS Nano*, 2021, **15**, 12286–12297, doi: 10.1021/acsnano.1c04091.

Author information

Deepka Rohila *has done his Ph.D. under the supervision of Dr. Savita Chaudhary from the Department of Chemistry Panjab University, Chandigarh, India. He received his master's degree from Department of Chemistry Panjab University, Chandigarh, India. His research interests mainly focus on the fabrication of advanced nanomaterials and their application in environmental remediation applications.*

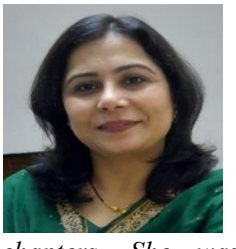

Savita Chaudhary *received her B.Sc, M.Sc and Ph.D. degrees in Chemistry from the Panjab University in Chandigarh, India. Dr. Chaudhary has published over 125 research articles in peer-reviewed international journals and 8 book chapters. She was awarded the DST-DAAD PPP fellowships in 2008. She is the recipient of prestigious Haryana Yuva Vigyan Ratan Award. She is an editorial member of the International Journal of Chemistry and Chemical Engineering (IJCCE) and Advanced Science, Engineering, and Medicine. She is also specialized in the modern analytical and spectroscopic techniques used for the characterizations and applications of semiconductor nanomaterials. Dr. Chaudhary is specialized in the synthesis, growth, properties, and applications of engineered nanostructures in the areas of gas, luminescent and biosensors, environmental remediation, catalysis, and photocatalysis. She has made significant contributions in the fields of surfactant chemistry and nanochemistry. Her recent work focuses on the design of different types of nanoparticles possessing higher biocompatibility applicable as carrier for herbicides.*

Ahmad Umar *received his Ph.D. in semiconductor and chemical engineering from Chonbuk National University, South Korea. He worked as a research scientist in Brain Korea 21, Centre for Future Energy Materials and Devices, Chonbuk National University, South Korea, in 2007–2008.*

© Engineered Science Publisher LLC 2021

Afterwards, he joined the Department of Chemistry in Najran University, Najran, Saudi Arabia. He is a distinguished professor of chemistry and served as deputy director of the Promising Centre for Sensors and Electronic Devices (PCSED), Najran University, Najran, Saudi Arabia. Professor Ahmad Umar is specialized in 'semiconductor nanotechnology', which includes growth, properties and their various high technological applications, for instance, gas, chemicals and biosensors, optoelectronic and electronic devices, field effect transistors (FETs), nanostructure-based energy-harvesting devices, such as solar cells, Li-ion batteries, super-capacitors, semiconductor nanomaterial- based environmental remediation, and so on. He is also specialized in the modern analytical and spectroscopic techniques used for the characterizations and applications of semiconductor nanomaterials. He contributed to the world of science by editing world's first handbook series on Metal Oxide Nanostructures and Their Applications (5-volume set, 3500 printed pages, www.aspbs.com/mona) and handbook series on Encyclopedia of Semiconductor Nanotechnology (7-volume set; www.aspbs.com/esn), both published by American Scientific Publishers (www.aspbs.com). He has published more than 600 research papers in reputed journal with h-index of 77 and i10-index of 379 with total citations of 20876 (According to Google scholar).

Publisher's Note: Engineered Science Publisher remains neutral with regard to jurisdictional claims in published maps and institutional affiliations.

 © Engineered Science Publisher LLC 2021